

ORIGINAL ARTICLE

How Stemlike Are Sphere Cultures From Long-term Cancer Cell Lines? Lessons From Mouse Glioma Models

Mushfika Ahmad, PhD, Karl Frei, PhD, Edith Willscher, PhD, Anja Stefanski, MSc, Kerstin Kaulich, PhD, Patrick Roth, MD, Kai Stühler, PhD, Guido Reifenberger, MD, Hans Binder, PhD, and Michael Weller, MD

Abstract

Cancer stem cells may mediate therapy resistance and recurrence in various types of cancer, including glioblastoma. Cancer stemlike cells can be isolated from long-term cancer cell lines, including glioma lines. Using sphere formation as a model for cancer cell stemness in vitro, we derived sphere cultures from SMA-497, SMA-540, SMA-560, and GL-261 glioma cells. Gene expression and proteomics profiling demonstrated that sphere cultures uniformly showed an elevated expression of stemness-associated genes, notably including *CD44*. Differences in neural lineage marker expression between nonsphere and sphere cultures were heterogeneous except for a uniform reduction of β -III-tubulin in sphere cultures. All sphere cultures showed slower growth. Self-renewal capacity was influenced by medium conditions but not nonsphere versus sphere culture phenotype. Sphere cultures were more resistant to irradiation, whereas both nonsphere and sphere cultures were highly resistant to temozolomide. Nonsphere cells formed more aggressive tumors in syngeneic mice than sphere cells in all models except SMA-560. There were no major differences in vascularization or infiltration by T cells or microglia/macrophages between nonsphere and sphere cell-derived tumors implanted in syngeneic hosts. Together,

these data indicate that mouse glioma cell lines may be induced in vitro to form spheres that acquire features of stemness, but they do not exhibit a uniform biologic phenotype, thereby challenging the view that they represent a superior model system.

Key Words: Expression profiling, Glioma stem cells, Murine glioma, Radiosensitivity, Stemness, Temozolomide.

INTRODUCTION

Glioblastomas are highly aggressive intrinsic brain tumors that may develop at all age groups, with incidence steadily increasing with age. Despite multimodal treatment of surgery followed by radiotherapy and alkylating agent chemotherapy, the median survival of glioblastoma patients is still in the range of less than 1 year in population-based studies (1). Effective treatments may be impeded by the high morphologic, phenotypic, and genetic cellular diversity.

A specific subpopulation of tumor cells, variably termed “glioma stem cells” or “glioma-initiating cells,” has been identified in human glioblastomas and has been proposed to confer therapy resistance and tumor progression despite multimodal therapy (2–4). Glioma stem cells are believed to be responsible for tumor initiation and growth because of their unlimited self-renewal capacity and the ability to give rise to more differentiated tumor cells in the tumor bulk. Furthermore, they have been proposed to express specific DNA damage response proteins as well as drug efflux proteins in response to radiotherapy and chemotherapy with DNA alkylating agents such as temozolomide (TMZ) (5–7).

Neural stem cell culture conditions have been used as a standard method to isolate and selectively expand glioma stem cells as tumor spheres that resemble neurospheres in culture not only from resected primary gliomas *ex vivo* but also from C6 rat and U373MG, A172, and U87MG human glioma cell lines (2–4, 8, 9). Reports on the size of the cell population isolated from the C6 rat glioma cell line that displayed these stem cell characteristics varied from 4% to 87% (9, 10). Similar to neural stem cells, the putative cancer stem cells from glioma cell lines have been shown to be capable of clonal growth, to exhibit multilineage differentiation potential, and to share the expression of various neural stem/progenitor cell markers, including CD133, nestin, Musashi-1, and Sox2 (8, 10–13). These neural stem cell characteristics as well as their *in vivo* tumorigenicity are among the criteria used to identify glioma stem cells.

From the Laboratory of Molecular Neuro-Oncology, Departments of Neurology (MA, PR, MW) and Neurosurgery (MA, KF); University Hospital Zurich, and Neuroscience Center (MA, KF, PR, MW), University of Zurich, Zurich, Switzerland; Interdisciplinary Institute for Bioinformatics, University of Leipzig, Leipzig, Germany (EW, HB); Molecular Proteomics Laboratory, Center for Biological and Medical Research (BMFZ) (AS, KS); Department of Neuropathology and German Cancer Consortium (DKTK), partner site Essen/Düsseldorf (KK, GR); and Institute for Molecular Medicine (KS), Heinrich Heine University, Düsseldorf, Germany.

Send correspondence and reprint requests to: Michael Weller, MD, Department of Neurology, University Hospital Zurich, Frauenklinikstrasse 26, CH-8091 Zürich, Switzerland; E-mail: michael.weller@usz.ch

This work was supported by the National Center of Competence in Research (NCCR) Neural Plasticity and Repair and the German Cancer Consortium (DKTK) within the joint funding program on next-generation molecular diagnostics of malignant gliomas.

Mushfika Ahmad, Karl Frei, Edith Willscher, Anja Stefanski, Kerstin Kaulich, Hans Binder, and Kai Stühler report no conflict of interest. Guido Reifenberger has received a research grant from Roche and honoraria for advisory boards from Roche and Merck Serono. Patrick Roth has received honoraria for advisory boards from Roche, Molecular Partners, and MSD. Michael Weller has received research grants from Bayer, Isarna, Merck Serono, MSD, and Roche and honoraria for lectures or advisory boards from Isarna, Magforce, Merck Serono, MSD, and Roche.

Supplemental digital content is available for this article. Direct URL citations appear in the printed text and are provided in the HTML and PDF versions of this article on the journal's Web site (www.jneuropath.com).

The best choice of experimental model for glioma research depends on the type of scientific question to be addressed (14). GL-261 and spontaneous mouse astrocytoma (SMA) cell lines are the most commonly used syngeneic mouse glioma models (15–17). Here, we systematically addressed the question of whether sphere cultures can be derived from these cell lines and whether these preferentially exhibit features of stemness, including enhanced self-renewal, stem cell marker expression, multilineage differentiation potential, resistance to radiotherapy and chemotherapy, and tumorigenicity *in vivo*.

MATERIALS AND METHODS

Materials

Temozolomide (parental grade 2577461) was kindly provided by MSD Switzerland (Zug, Switzerland). Primary antibodies for flow cytometry included anti-human/mouse CD44 (working dilution of 1:100; eBiosciences, San Diego, CA), mouse anti-prominin (CD133)-1-phycoerythrin (1:100; Miltenyi Biotec, Bergisch Gladbach, Germany), mouse IgG2b_k isotype control (eBiosciences), phycoerythrin-conjugated mouse IgG isotype control (BD Biosciences, San Jose, CA), and fluorescein isothiocyanate-conjugated goat anti-rat IgG (BD Biosciences). The concentrations of isotype controls were adjusted to have the same IgG concentration as the specific antibodies. For immunofluorescence staining, the following primary antibodies were used: monoclonal mouse anti-nestin IgG1 (1:200) (AbD Serotec, Düsseldorf, Germany), polyclonal rabbit anti-Musashi-1 (1:400; Chemicon, Zug, Switzerland), polyclonal rabbit anti- β -III-tubulin (β III_T) IgG (1:1000; Abcam, Cambridge, UK), monoclonal mouse anti-2',3'-cyclic-nucleotide 3'-phosphodiesterase (CNPase) IgG1 (1:100; Chemicon), polyclonal rabbit anti-glial fibrillary acidic protein (GFAP) IgG (1:1000; Dako, Baar, Switzerland), and monoclonal rabbit anti-Ki-67 IgG (1:100; Epitomics, Nunningen, Switzerland). Alexa Fluor-488-conjugated goat anti-rabbit IgG (Invitrogen, Basel, Switzerland) or anti-mouse IgG (Invitrogen) (both 1:100) were used as secondary antibodies. For immunohistochemistry of mouse gliomas *in vivo*, the following primary antibodies were used: anti-human/mouse CD44 (1:1000; eBiosciences), polyclonal rabbit anti- β III_T IgG (1:1000; Abcam), rat anti-CD3 (1:1000; BD Biosciences), anti-CD11b (1:1000; BD Biosciences), anti-CD31 (1:50; BD Biosciences), and anti-Ki-67 (1:100; Epitomics).

Cell Culture

Murine SMA-497, SMA-540, and SMA-560 cells were kindly provided by Dr D. D. Bigner (Durham, NC). GL-261 cells were obtained from the American Type Culture Collection (Rockville, MD). These cell lines are commonly cultured as adherent monolayers in Dulbecco modified Eagle medium (Gibco, Life Technologies, Zug, Switzerland) supplemented with 10% heat-inactivated fetal calf serum (Biochrom KG, Zug, Switzerland) and 2 mmol/L glutamine (Biochrom KG) (DM medium), herein referred to as “nonsphere” cultures. Sphere cultures were generated from nonsphere cultures by placing the cells in Neurobasal (NB)-A medium (Gibco) supplemented with 2% B27 (Gibco), 20 ng/mL basic fibroblast

growth factor, 20 ng/mL epidermal growth factor (Peprotech, London, UK), 6.3 U/mL heparin (Sigma, St Louis, MO), and 2 mmol/L glutamine (NB medium) at a density of 50,000 cells/mL. Sphere cultures were cultured until the third passage before use for experiments, with a passage duration of approximately 7 days.

Cell Growth and Doubling Times

Nonsphere (2,000/mL) or sphere (20,000/mL) cells were seeded in 25-cm² flasks (TPP Techno Plastic Products AG, Trasadingen, Switzerland) in their respective medium. Everyday for nonsphere and every 2 days for sphere cultures, an aliquot of the cells was dissociated into single-cell suspensions using TrypLE Express cell dissociation reagent (Gibco) and stained with 0.4% Trypan blue; viable cells were counted using Neubauer chambers (VWR International AG, Dietikon, Switzerland). Cell counts from 3 separate experiments were obtained.

Limiting Dilution Assay

Nonsphere cells were seeded in duplicate in 0.5 mL DM medium in 24-well plates (Faust Laborbedarf AG, Schaffhausen, Switzerland) at the following cell numbers per well: 250, 83, 28, 9, 3, and 1. Sphere cells were also seeded in duplicate in 0.5 mL NB medium at the following cell numbers per well: 1,000, 250, 63, 16, 4, and 1. A “colony” was defined by more than 25 nonsphere cells; the colonies were counted at 4 to 14 days. A “sphere” was defined by more than 5 cells, and the number of spheres was counted after 7 to 20 days. A 10 \times solution of growth factors (epidermal growth factor and fibroblast growth factor) and heparin was added to the sphere culture plates to a final concentration of 20 ng/mL of growth factors and 6.3 U/mL of heparin, respectively, every week. To assess the plasticity of nonsphere and sphere cells, the colony-forming and sphere-forming capabilities were also assessed in limiting dilution assays after a switch of conditions, that is, by seeding sphere cells in DM medium and by seeding nonsphere cells in NB medium at the cell numbers indicated above for the respective medium. Results were derived from 3 separate experiments.

Clonogenicity Assays

Nonsphere or sphere cells were seeded at 1,000 cells per well with 5 replicates in 96-well plates, treated as indicated and then further cultured until the untreated nonsphere cells had formed colonies and the sphere cultures had reached 100 to 150 μ m in sphere size. Growth factors were supplemented weekly to the NB medium as previously described. Then, alamarBlue (Invitrogen) was added to the plates and incubated for 4 hours at 37°C, after which the plates were analyzed using a cytofluorometer (Infinite 200PRO, Tecan Group Ltd, Männedorf, Switzerland). Assays were repeated 3 times. Appropriate control experiments had indicated that the alamarBlue assay is a reliable surrogate marker of clone or sphere number but more convenient for high-volume pharmacologic studies than actual clone or sphere counting.

Flow Cytometry

Cells were harvested and dissociated into single cells by TrypLE Express cell dissociation reagent and resuspended in phosphate PBS containing 0.5% fetal calf serum and 2 mmol/L

ethylenediaminetetraacetic acid (FACS buffer). Cells were stained with primary antibodies for 30 minutes on ice in the dark. After washing with PBS, cells were resuspended in FACS buffer and stained with secondary antibody (when required) on ice for 30 minutes. After staining, cells were washed with PBS, resuspended in FACS buffer, and analyzed using the Beckman Coulter and Summit 4.3 software (Nyon, Switzerland). Staining intensity was expressed as specific fluorescence indexes derived by dividing signal obtained with specific as opposed to isotype control antibody. Percentages of positively stained cells were measured by setting the gate at 1.3% of the fluorescence (represented by the FL 1 log in the histogram) of the isotype control. Similar results were obtained from 2 separate flow cytometric analyses.

Immunofluorescence Microscopy

To analyze the expression of neuronal stem cells and mature neuronal and glial cell markers, sphere cultures were prepared as cytospin samples whereas nonsphere cultures were grown on sterilized 11-mm glass coverslips (Assistent 1001/12) coverslips at 5,000 cells in a 24-well plate until they were 80% to 90% confluent. Spheres that had reached a size of 150 to 200 μm in diameter were harvested by centrifugation at 700 rpm for 5 minutes and resuspended in 1,200 μL of NB medium. One hundred microliters of resuspended spheres were cytospun using the Cytospin 4 (Thermo Scientific, Wohlen, Switzerland) at 650 rpm for 4 minutes. Cytospun spheres were left to dry for 15 minutes and fixed and stained as outlined below. Cells were washed in PBS and fixed at room temperature for 10 minutes in either 4% paraformaldehyde or methanol precooled to -20°C , according to the antibody recommendations. After washing, cells fixed in paraformaldehyde were permeabilized in 0.1% Triton X-100 in PBS for 10 minutes. Cells were then washed and blocked using blocking solution (Candor Biosciences, Wangen, Germany) for 25 minutes. Primary antibodies were prepared in antibody dilution buffer (DCS Innovative Diagnostik System, Hamburg, Germany). Cells were stained with primary antibodies for 90 minutes. After staining, cells were washed in PBS and stained using secondary antibodies prepared in antibody dilution buffer for 30 minutes. Cells were then stained with 1 $\mu\text{g}/\text{mL}$ 4',6-diamidino-2-phenylindole (Invitrogen) at a working dilution of 1:1000 in antibody dilution buffer for the last 10 minutes. Finally, the cells were washed in PBS and mounted on microscope slides (Superfrost Plus; Thermo Scientific) using fluorescent mounting medium (Dako). Analysis was performed using the SP5 laser scanning confocal microscope (Leica, Wetzlar, Germany) and LAS-AF Lite software. Positively stained cells were identified by setting the fluorescence signal intensity used for the positive control for each antibody staining under saturation levels. The P19 neuronal progenitor cell line was used as a positive control for nestin and Musashi-1; cryosections of wild-type C57BL/6 mouse brain were used as positive control for GFAP, β IIIIT, and CNPase.

Irradiation

Cells were seeded in 0.5 mL medium into 24-well plates for limiting dilution or 96-well plates for clonogenic survival assays. On the next day, the plates were irradiated at 0, 1, 3, or 9 Gy using a Co source (Gebrüder Sulzer, Thermische

Energiesysteme, 60-Co, Winterthur, Switzerland). Cells were allowed to grow, and colonies or spheres were counted at 4 to 14 days after seeding when colonies of at least 25 nonsphere cells had formed or at 7 to 20 days after seeding when spheres of at least 5 sphere cells had formed; alternatively, alamarBlue assays (Invitrogen) were performed.

TMZ Exposure

Cells were seeded in 0.5 mL of their respective medium and plated into 24-well plates for limiting dilution assays or 96-well plates for clonogenic survival assays. On the next day, the cells were treated with 0 (serum-free), 10, 100, or 1,000 $\mu\text{mol}/\text{L}$ TMZ diluted in serum-free DM medium or complete NB medium for 24 hours. The cells were then cultured in fresh complete DM or NB medium and allowed to grow. Colonies or spheres were counted, or alamarBlue assays were performed as previously described.

In Vivo Experiments

The standard operating procedure and the treatment of all animals were according to the Swiss Cantonal Veterinary office regulations under the Animal license permission no. 95/2009 and 235/2012. After anesthesia, a burr hole was drilled in the skull 2 mm lateral to the bregma. The needle of a Hamilton syringe (Hamilton, Darmstadt, Germany) was introduced to a depth of 3 mm. A volume of 2 μL of PBS single-cell suspension was slowly injected into the right striatum. One thousand nonsphere or sphere cells of SMA-497, SMA-540, or SMA-560 cell lines were implanted into 6 groups of 11 VM/Dk mice per group. Similarly, GL-261 cells were implanted in 2 groups (nonsphere and sphere cells) of 10 C57BL/6 mice per group. Two mice per group were killed using a pre-randomization scheme when any mouse in the experiment became symptomatic to perform histologic studies to assess tumor growth at an early stage (Table). The other 9 mice (8 mice for the GL-261 model) were killed when they displayed neurologic signs and were thus used for survival analysis (pooled from 2 separate experiments). These, along with the rest of the brains collected at termination of the experiment (Day 80 after implantation), were used for further immunohistochemical analyses. All brains collected after the mice were killed were embedded in cryomolds in Shandon Cytochrome yellow (Thermo Scientific) and frozen in liquid N_2 . Tumor incidences were determined using hematoxylin and eosin-stained 8- μm -thick cryosections cut using the Microm HM560 (Microchom HM560; Thermo Scientific) before constructing and analyzing Kaplan-Meier survival curves using the logrank test in GraphPad Prism 5.0 software (GraphPad, La Jolla, CA).

Immunohistochemical Analysis

Cryosections were fixed in ice-cold acetone for 10 minutes, washed in PBS, and treated with 3% H_2O_2 for 10 minutes. The sections were then washed and blocked using blocking solution (Candor Biosciences). After blocking, the primary antibodies were applied overnight at 4°C . Next, the sections were washed and probed using biotinylated rabbit-anti-rat secondary antibody (Vector) for 30 minutes at room temperature. The antigen antibody conjugates were then detected by staining with 3,3'-diaminobenzidine (Dako) for 1 to 3 minutes.

TABLE. Characterization of Nonsphere and Sphere Cell-Derived Tumors In Vivo

	SMA-497		SMA-540		SMA-560		GL-261	
	Nonsphere	Sphere	Nonsphere	Sphere	Nonsphere	Sphere	Nonsphere	Sphere
Early stage								
Median survival (days) (mean ± SE)	14 ± 0.13	>80	>80	>80	>80	15 ± 0.15	35 ± 0.53	73 ± 2.2
Tumor incidence, n/all, %	23/23 (100)	1/7 (14)	3/7 (43)	0/7 (0)	2/4 (50)	13/14 (93)	4/4 (100)	4/4 (100)
Tumor diameter, mm	2.8 ± 0.1	0.17	0.7 ± 0.04	n/a	0.85 ± 0.11	3.9 ± 0.20	3 ± 0.49	3.7 ± 0.35
Late stage								
Tumor incidence, n/all, %	n/a	5/14 (36)	9/16 (56)	1/16 (6)	6/13 (46)	None	8/16, 50	8/14, 57
Mean tumor diameter, mm	n/a	1.6 ± 0.05	3.9 ± 0.32	3.7	2.9 ± 0.5	n/a	4.0 ± 0.21	3.1 ± 0.31
Infiltration into contralateral hemisphere	Yes	No	Yes	No	No	Yes	Yes	Yes
Multifocal tumors (multifocal/total tumors, %)	6/20, 30	0	3/8, 37.5	0	No	4/18, 22.2	4/18, 22.2	5/18, 27.8
Ki-67 mean ± SE, %	27.7 ± 5.8	23.2 ± 0.76 p = 0.43	62.1 ± 1.68	42.1 ± 4.75	55.6 ± 1.67	68.9 ± 5.4* p = 0.019	30.6 ± 3.71	50.2 ± 3.56 * p = 0.032
Ki-67 distribution within tumor	More at tumor periphery	n/a tumor too small	Uniform	Uniform	Uniform	Uniform	Uniform	Uniform
CD31 count (mean ± SE)	42.8 ± 2.97	44.4 ± 2.62 p = 0.70	41.5 ± 1.63	39 ± 0.49	86 ± 2.59	97.3 ± 4.32* p = 0.011	47 ± 2.05	44.6 ± 2.91 p = 0.20
CD3 count (mean ± SE)	451 ± 69.7	155 ± 40.1*** p = 0.00036	88.4 ± 36.6	67.5 ± 36.3	122 ± 46.3	113 ± 41.1 p = 0.07	178 ± 23.9	359 ± 51.3** p = 0.03
CD11b count (mean ± SE)	1,816 ± 159	1,015 ± 142** p = 0.0014	1,927 ± 180	1,436 ± 76	1,386 ± 133	1,048 ± 56 p = 0.14	783 ± 68	1,334 ± 139* p = 0.032

SMA-497 nonsphere and SMA-560 sphere groups reached the terminal stage at Day 14 (early stage) after implantation. To assess tumor morphology at progression, 2 to 3 mice per group were killed in the other SMA groups. Results from 2 pooled experiments are included. Two mice per group were also killed in the GL-261 studies at the occurrence of first signs on Day 29. The remainder of the data included tumors that developed after Day 14 up to and including the termination of the experimental Day 80 after implantation (late stage). Quantitative data for Ki-67 stained cells are represented as the mean percentage of positive cells of the total along with the SE values. Quantification of blood vessel density (CD31), T cells (CD3), and microglia/macrophages (CD11b-positive) are expressed as the mean and SE of positively labeled cells (* p < 0.05, ** p < 0.01, *** p < 0.001, paired *t*-test with unequal variance caused by heterogeneity within tumor areas). For all immune-labeled stainings, the cells were counted from 4 to 6 different areas (depending on tumor size) within the tumor from 3 different tumors (with the exception of the SMA-540 subline) each at the terminal stage in an area of 0.35 mm². All counts from all animals were derived to obtain the mean and SE. SMA-540 sphere cells were least tumorigenic. Because of the occurrence of only 1 incidence of tumor, statistical comparison between the nonsphere and sphere groups could not be made for all stainings done.

The nuclei were stained using hematoxylin for 4 minutes, washed in water, and dehydrated twice in 96% ethanol, then twice in 100% ethanol and 3 times in xylol before mounting onto coverslips using Eukitt mounting medium. Quantification of proliferating cells (Ki-67), blood vessel density (CD31), T cells (CD3), and microglial cells/macrophages (CD11b) was obtained from 4 to 6 different areas (depending on tumor size) from 3 tumors each at the terminal stage in an area of 0.35 mm². Beta-III-tubulin and CD44 levels were not quantified. Statistical significance was calculated using the paired Student *t*-test.

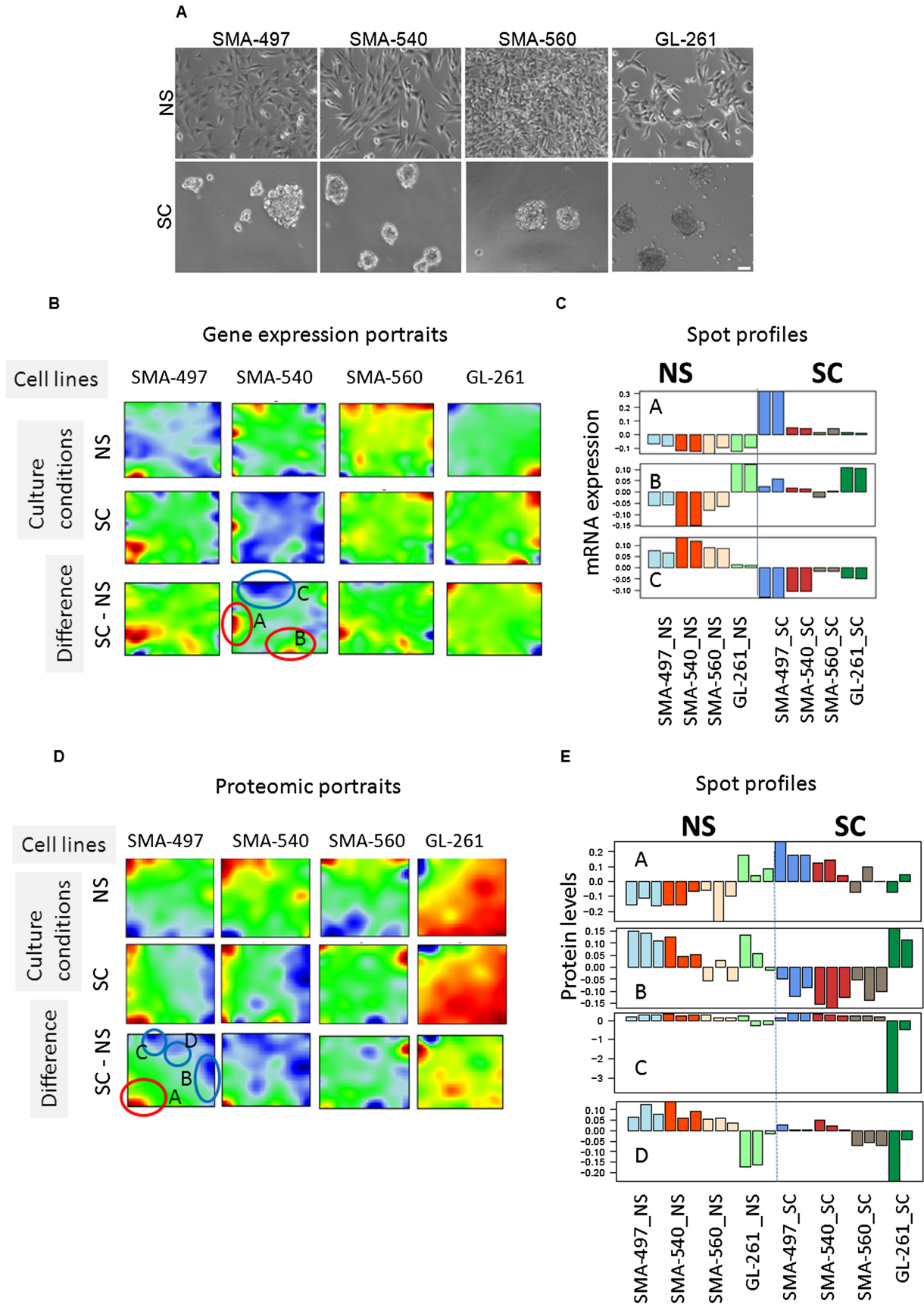
Analysis of Gene Expression and Proteomics Data

The generation of transcriptomic and proteomic data is reported in detail in Methods, Supplemental Digital Content 1, <http://links.lww.com/NEN/A663>. Raw microarray data were calibrated and summarized using the RMA method including quantile normalization (18, 19). The expression value of each gene was transformed into log10 scale and centered with respect to its mean value averaged over all samples investigated (20). A relative log expression value of zero indicates that the gene is expressed according to its mean expression value, whereas positive and negative values refer to overexpression and underexpression in the data set, respectively.

Gene expression was analyzed using the portraying method based on self-organizing map (SOM) data compression.

This approach transforms the gene expression patterns of more than 20,000 genes per sample into intuitive quadratic mosaic portraits representing 50 × 50 grids, in which each tile refers to 1 microcluster of concertedly expressed genes called “metagene” (20, 21). Further analyses were performed either in metagene space, for example, by clustering concertedly expressed metagenes into so-called spot modules, by calculating group-averaged mean portraits for each cell line and sample condition, or by selecting differential features by calculating difference portraits (Figure, Supplemental Digital Content 2, <http://links.lww.com/NEN/A664> and Figure, Supplemental Digital Content 3, <http://links.lww.com/NEN/A665>) or based on single-gene expression data, for example, by applying gene set enrichment analysis for functional interpretation. The latter approach makes use of the gene set enrichment score (GSZ), which estimates the significance of differential expression of the members of a set of genes compared with the mean expression of all genes in a sample (22). Gene sets were taken from standard gene ontology categories or from previous publications as indicated below. All analyses were performed using the R-program opoSOM providing basic SOM portraying in combination with a series of data mining methods and comprehensive visualization options (20, 22).

Protein data were processed using the same analysis pipeline as previously described for gene expression data



except for RMA calibration, that is, the data were log10 transformed, centralized, and subsequently analyzed using the SOM-portraying method. Suitability of this method for analyzing proteomics data was recently demonstrated (23).

Statistical Analysis

For the functional assays, data are usually representative of experiments performed 3 times with similar results. Statistical significance for the clonogenicity studies after irradiation or TMZ treatments was assessed with a 2-way analysis of variance test using the GraphPad Prism 5.0 software. Statistical analysis of cell doubling time and immunofluorescence was calculated using 2-tailed Student *t*-test with equal variance whereas immunohistochemistry data were analyzed using 2-tailed Student *t*-test with unequal variance because of the heterogeneous nature of tumors. Survival statistics in the *in vivo* studies were calculated using the logrank test from the GraphPad Prism 5.0 software.

RESULTS

Gene Expression and Proteomics Profiling of Sphere Versus Nonsphere Cultures of Murine Glioma Cells In Vitro

Sphere cultures were established from nonsphere cultures of all 4 mouse glioma cell lines by switching the nonsphere cultures to NB medium, which resulted in sphere formation in all cell lines (Fig. 1A). These spheres could be maintained for months under these culture conditions. Microarray-based mRNA expression profiling and mass spectrometry-based proteome analyses were done to assess the gene activity in terms of mRNA and protein abundance, respectively (Methods, Supplemental Digital Content 1, <http://links.lww.com/NEN/A663>). The primary analysis was performed by comparing the expression portraits of all sample classes (i.e. cell lines and culture conditions) obtained from the transcriptome and proteome data, respectively. In contrast to light microscopic features, which were dominated by culture conditions, molecular expression landscapes were mainly governed by the respective cell line (Fig. 1B). For example, each of the SMA lines showed similar gene expression largely independent of the nonsphere or sphere culture condition, reflected also in the similarity tree based on mRNA expression profiles, which also outlines that SMA-560 is less related to the other 2 more related SMA lines (Figure, Supplemental Digital Content 4, <http://links.lww.com/NEN/A666>). The proteomic portraits supported this observation for GL-261, whereas the proteomics portraits of the SMA samples revealed clear differences between the sphere culture and nonsphere culture conditions (Fig. 1D, E; Figure, Supplemental Digital Content 5, <http://links.lww.com/NEN/A667>). Nonsphere cultures of the SMA lines were similar, whereas GL-261 exhibited a different proteomics profile. Thus, altogether, the similarities

between paired nonsphere and sphere cultures were higher than among nonsphere versus sphere cultures, irrespective of whether GL-261 was included or excluded from the analyses.

Expression of Stemness Markers

We next performed differential analyses between the samples cultured under nonsphere versus sphere conditions (Figure, Supplemental Digital Content 2, <http://links.lww.com/NEN/A664> and Figure, Supplemental Digital Content 3, <http://links.lww.com/NEN/A665>). Both transcriptomics and proteomics data revealed a cluster of mRNA and proteins concertedly downregulated in nonsphere and upregulated in sphere cultures (depicted as spot profiles in Fig. 1C, E). Selected sets of human embryonic stem cell marker genes (24) were selectively upregulated in sphere cultures at the mRNA level and even more clearly at the protein level (Fig. 2). No such changes were observed for other marker sets (data not shown). Changes in stem cell marker expression induced by sphere formation were often not uniform: Notch1 mRNA was upregulated in SMA-560 (expression fold change [FC] = 1.8; $p = 0.06$); Sox2 mRNA in SMA-497 (FC = 1.8; $p = 0.05$), SMA-540 (FC = 2.2; $p = 0.005$), and SMA-560 (FC = 3.3; $p = 0.001$); and $\alpha 6$ -integrin mRNA in SMA-497 (FC = 3.1; $p = 0.04$). Alpha-6-integrin protein was increased in SMA-497 (FC = 1.5; $p = 0.07$), SMA-540 (FC = 1.5; $p = 0.02$), and SMA-560 (FC = 1.8; $p = 0.03$). CD44 induction as a marker of stemness in sphere cultures was confirmed by flow cytometry (Fig. 3A). Apart from SMA-497 nonsphere and sphere cultures, the mouse glioma cell lines were negative for CD133, and CD133 expression decreased when SMA-497 cells were shifted to sphere culture conditions (Fig. 3B). There was also heterogeneous expression of a third stem cell marker, nestin, among nonsphere and sphere cultures: nestin expression decreased in SMA-540 ($p = 0.0047$), increased by trend in SMA-560 ($p = 0.16$), and remained similar in the other 2 cell lines (Fig. 3C, D). Finally, Musashi-1 was highly expressed in 3 of the 4 cell lines and essentially unaffected by switching from nonsphere to sphere culture conditions (Fig. 3E, F).

Expression of Neuroglial Differentiation Markers

The nonsphere cultures expressed neuroglial differentiation markers at variable levels by immunofluorescence microscopy. The astrocyte marker GFAP was highly expressed in SMA-497 and SMA-560, to a lesser degree in GL-261, but not in SMA-540 (Fig. 4A, B). The neuronal marker β IIIIT was expressed in the SMA lines, but only at a very low level in GL-261 (Fig. 4C, D). In contrast, the oligodendroglial marker CNPase was almost uniformly expressed (Fig. 4E, F). The percentages in Figure 4B, D, and F illustrate that many cells coexpressed different markers of the different neuroglial lineages. We then determined whether induction of the sphere culture phenotype was associated with decreased expression

FIGURE 1. Gene expression and proteomic profiling of sphere cultures derived from long-term mouse glioma cell (SMA) lines *in vitro*. **(A)** Light microscopic features under nonsphere and sphere culture conditions. **(B, C)** Expression profiling: Mean self-organizing map (SOM) gene expression portraits of the cell lines cultured under nonsphere or sphere conditions and of the cell line-specific difference between nonsphere and sphere cultures. The ellipses in the difference portrait of SMA-540 indicate clusters of genes (so-called spots), which are differentially expressed between nonsphere and sphere cultures **(B)**. Their expression levels in the different samples are shown as bar plots in **(C)**. Corresponding proteomics portrait **(D)** and spot profile **(E)** results for proteomics. NS, nonsphere cultures; SC, sphere cultures.

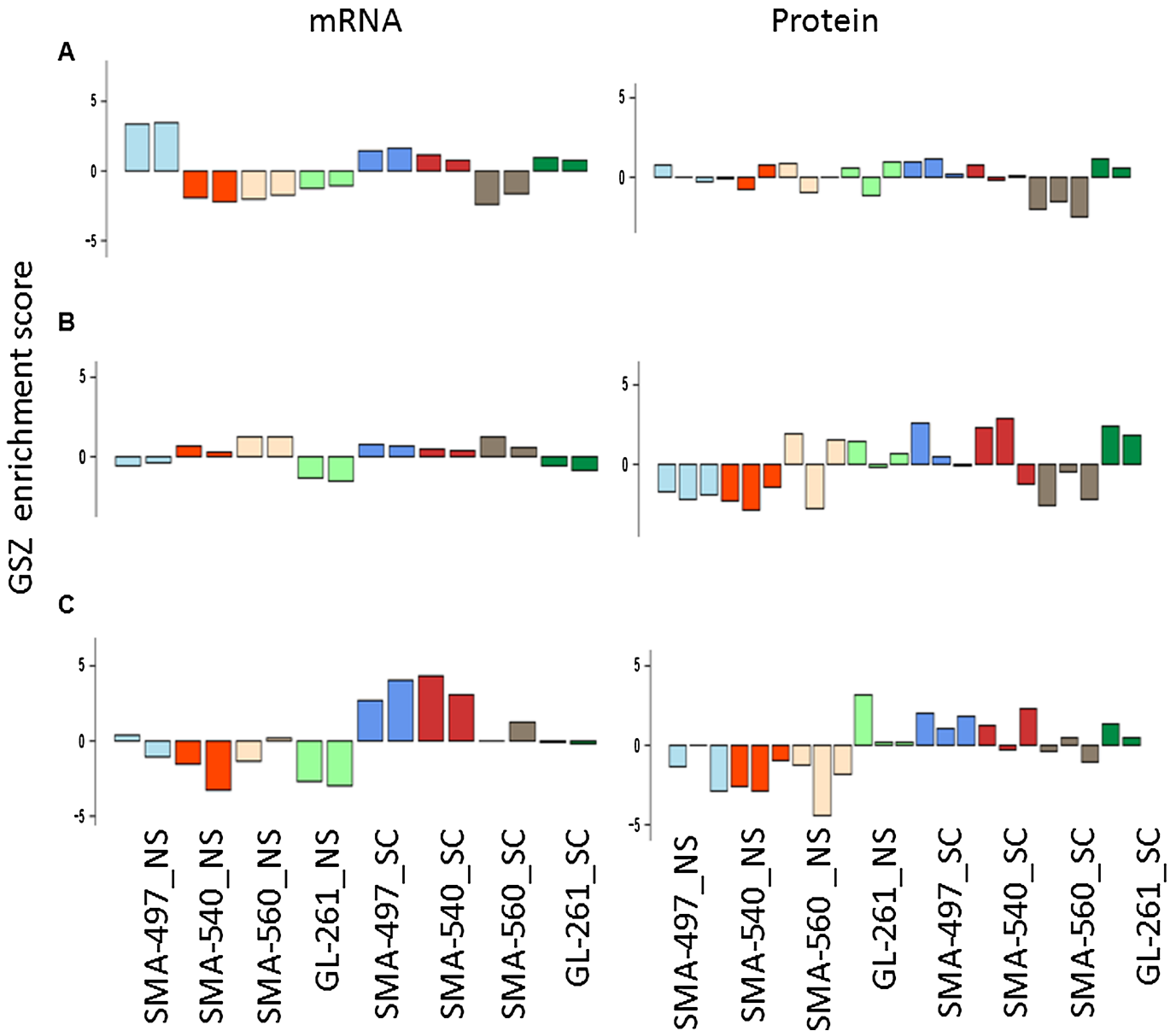


FIGURE 2. Stem cell marker expression: Gene expression and proteomic profiling. Gene set enrichment analysis using stemness-related genes (24) shows profiles of the enrichment score for 3 gene sets in all cell systems studied. The sets contain genes differentially upregulated in hESC9 (**[A]** set hESC9), abundant in hESC (**[B]** hESC10), and myc-regulated targets (**[C]** myc2). NS, nonsphere cultures; SC, sphere cultures; hESC, human embryonic stem cell marker genes.

of these markers. Glial fibrillary acidic protein increased under sphere culture conditions in SMA-540 ($p = 0.0007$) and by trend in GL-261 ($p = 0.18$), whereas CNPase remained highly expressed throughout. Only β IIIIT expression uniformly decreased when the cells were induced to undergo sphere formation at the following significance levels: SMA-497 ($p = 0.0009$), SMA-540 ($p = 0.034$), SMA-560 ($p = 0.13$), and GL-261 ($p = 0.093$).

Cell Growth and Clonogenicity of Nonsphere Versus Sphere Cultures

Nonsphere cultures of the SMA cell lines had shorter doubling times than sphere cultures at the indicated signifi-

cance levels: SMA-497 ($p = 0.03$), SMA-540 ($p = 0.025$), SMA-560 ($p = 0.028$). The difference was not significant in GL-261 cells ($p = 0.067$) (Figure, Supplemental Digital Content 6, parts A–C, <http://links.lww.com/NEN/A668>). Also, quantification of the proliferation marker Ki-67 immunolabeling confirmed higher proliferation of nonsphere cultures for SMA-497 ($p = 0.019$), SMA-540 ($p = 0.005$), and SMA-560 ($p = 0.015$), but not for GL-261 ($p = 0.3$) (Figure, Supplemental Digital Content 6, parts D, E, <http://links.lww.com/NEN/A668>). The GSZ score of the gene set “cell division,” taken from the collection of gene ontology terms “biological process,” in all systems studied confirmed this result at least by trend at the proteomics level: nonsphere conditions were associated with

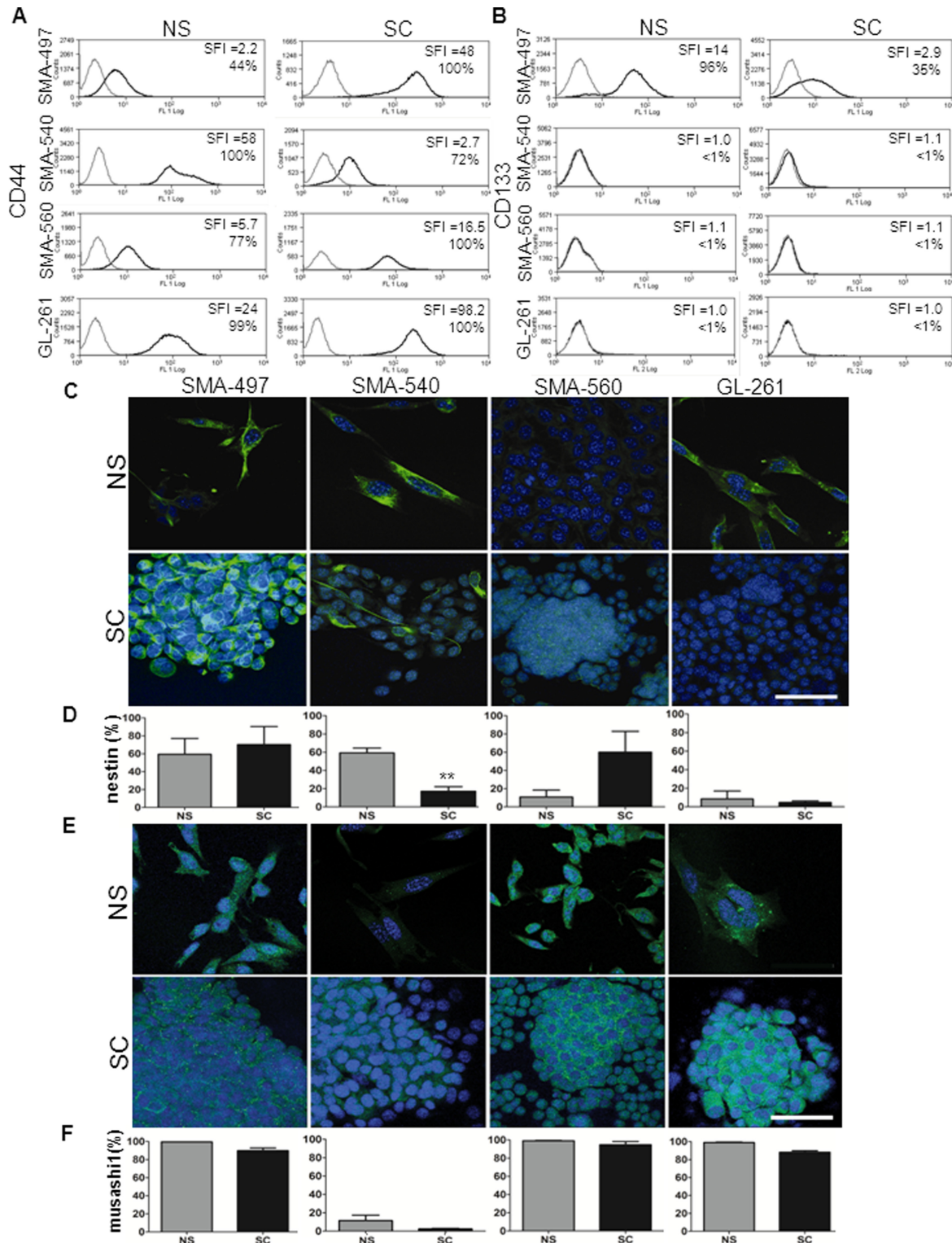


FIGURE 3. Stem cell marker expression: Candidate approach. CD44 (**A**) or CD133 (**B**) expression was assessed by flow cytometry (CD44/CD133, black lines; isotype control, gray lines, representative of experiments done twice with similar results). Specific fluorescence index (SFI) and percentages of positive cells are indicated in the right upper corner of each graph. Nestin (**C, D**) or Musashi-1 (**E, F**) expression was determined by immunofluorescence microscopy and quantified based on 4',6-diamidino-2-phenylindole counterstaining from 3 separate stainings (* $p < 0.01$, paired t -test with equal variance). Scale bar = (**C, E**) 50 μ m. NS, nonsphere cultures; SC, sphere cultures.

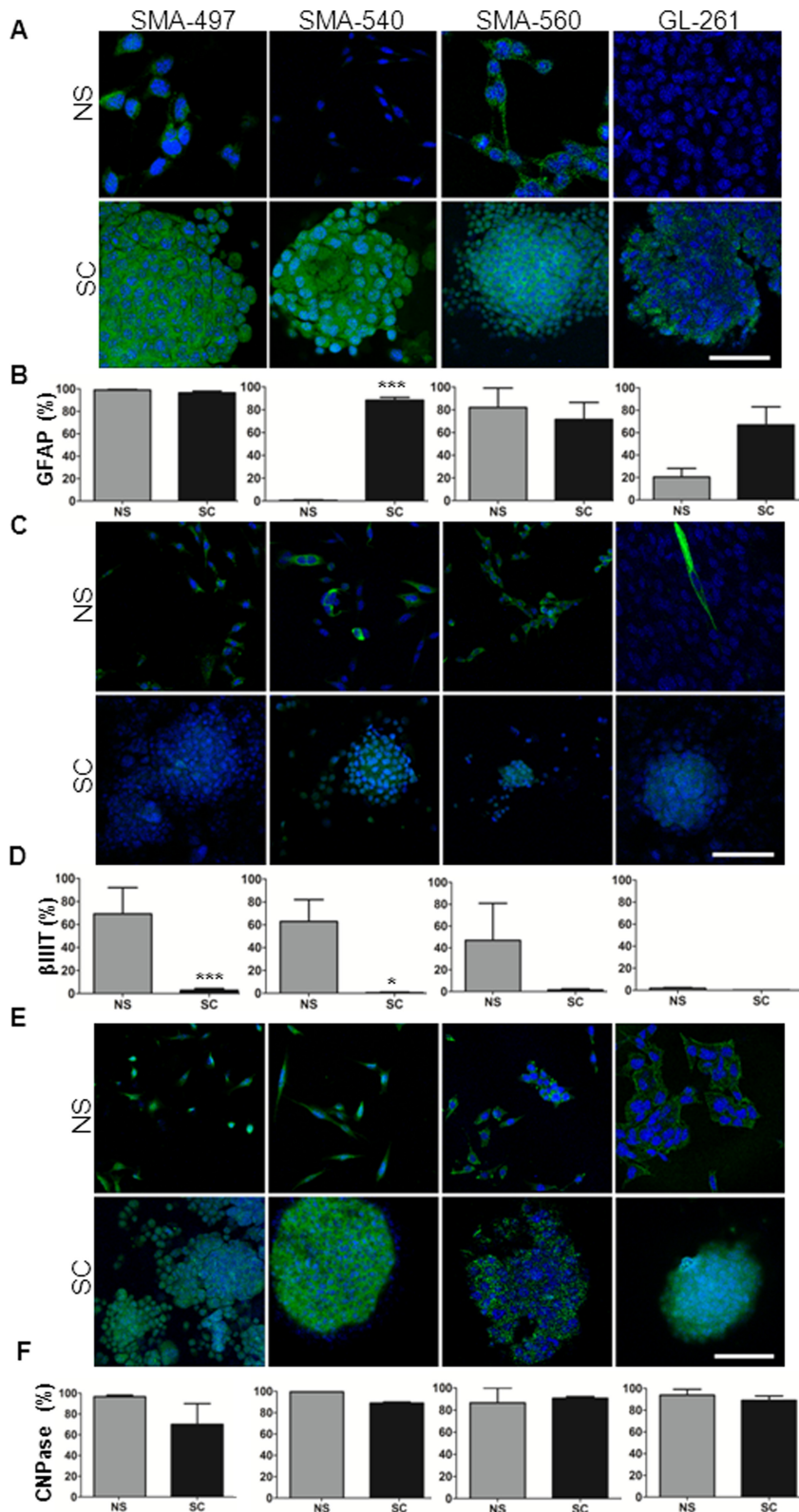


FIGURE 4. Neuroglial differentiation marker expression. Immunofluorescence microscopy was used to assess glial fibrillary acidic protein (GFAP) (**A, B**), β -III-tubulin (β IIIIT) (**C, D**), or 2',3'-cyclic-nucleotide 3'-phosphodiesterase (CNPase) (**E, F**) expression (nonsphere gray bars, sphere black bars; scale bar = 50 μ m). Quantitative analysis displays the mean and SD from 3 experiments (* $p < 0.05$, *** $p < 0.001$, paired t -test with equal variance). NS, nonsphere cultures; SC, sphere cultures.

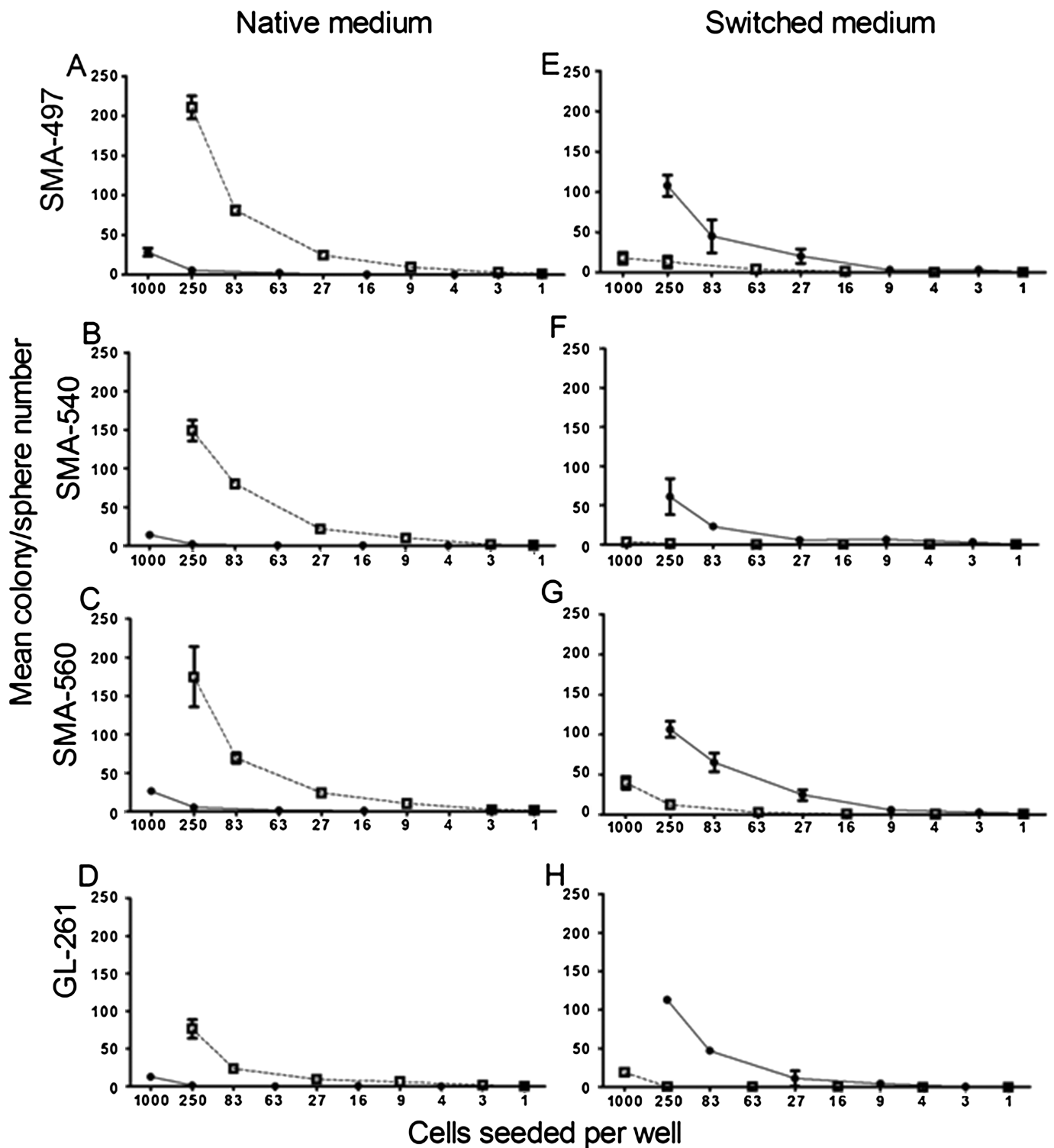


FIGURE 5. Clonogenicity and spherogenicity of nonsphere versus sphere cells in vitro. **(A–H)** Colony numbers of nonsphere cultures (open squares, dotted lines) or sphere numbers of sphere cultures (black circles, straight lines) were obtained from 3 limiting dilution assays at 4 to 14 days after seeding either in their native medium (DM medium [see Materials and Methods] for nonsphere and Neurobasal [NB] A medium for sphere cultures) **(A–D)** or in switched medium (nonsphere cells in NB medium and sphere cells in DM medium) **(E–H)**.

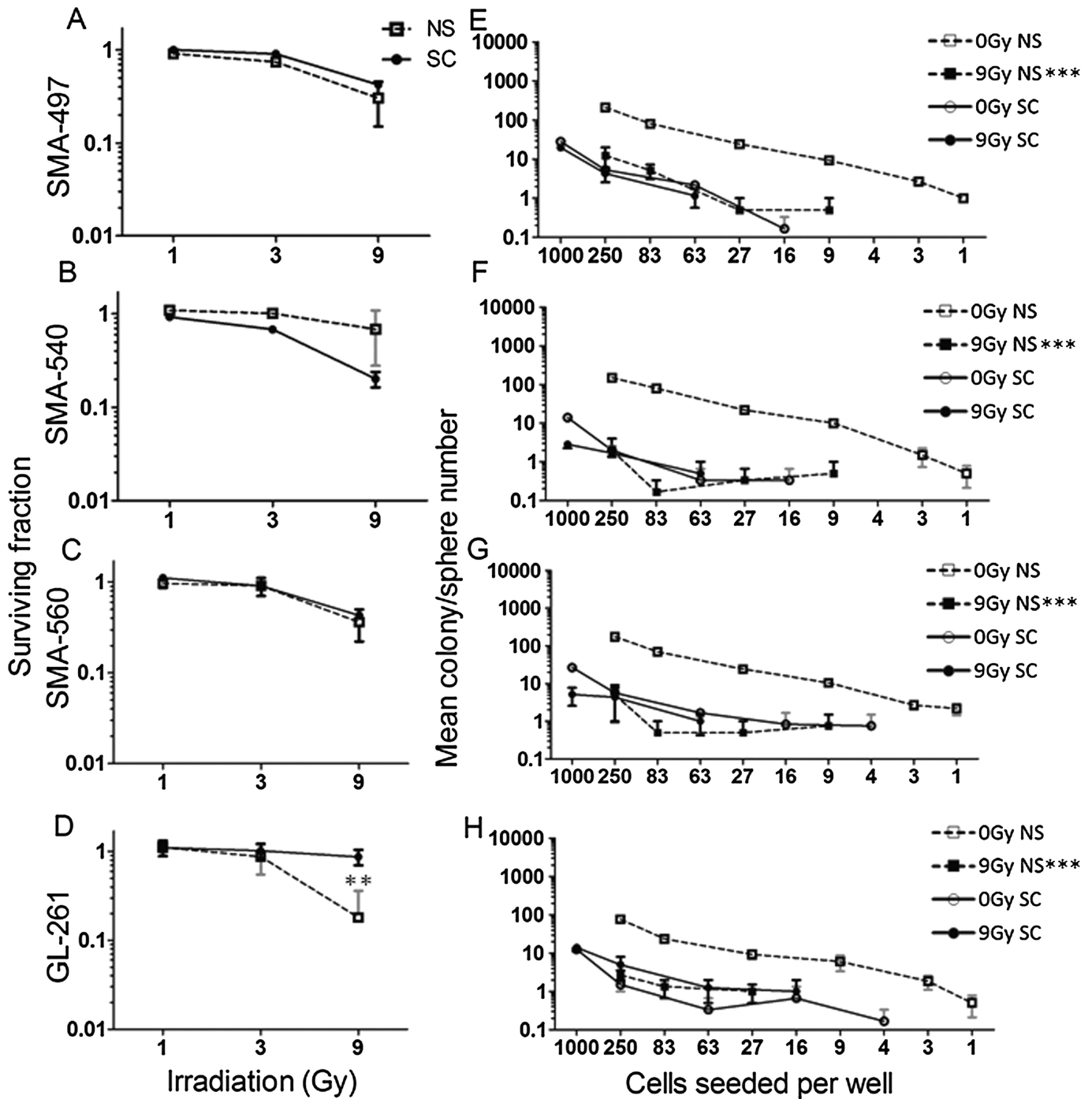


FIGURE 6. Radiosensitivity of nonsphere versus sphere cells in vitro. **(A–D)** The effect of 0, 1, 3, and 9 Gy of ionizing irradiation on the proliferation of nonsphere (open squares, dotted lines) versus sphere (filled circles, black lines) cells was assessed by irradiating 1,000 cells plated on 96-well plates and allowing them to recover for 5 to 14 days in 3 separate experiments. Assays were stopped when untreated cells became confluent. Quantification of cell density was done by alamarBlue staining. **(E–H)** Limiting dilution assays after irradiation at 0 (open squares, dotted line for nonsphere cells, open circle continuous line for sphere cells) or 9 Gy (closed square, dotted line for nonsphere cells, closed circle, continuous line for sphere cells) were performed. Colonies or spheres were counted 7 to 20 days after irradiation (n = 3, * p < 0.05, *** p < 0.001, 2-way analysis of variance). NS, nonsphere cultures; SC sphere cultures.

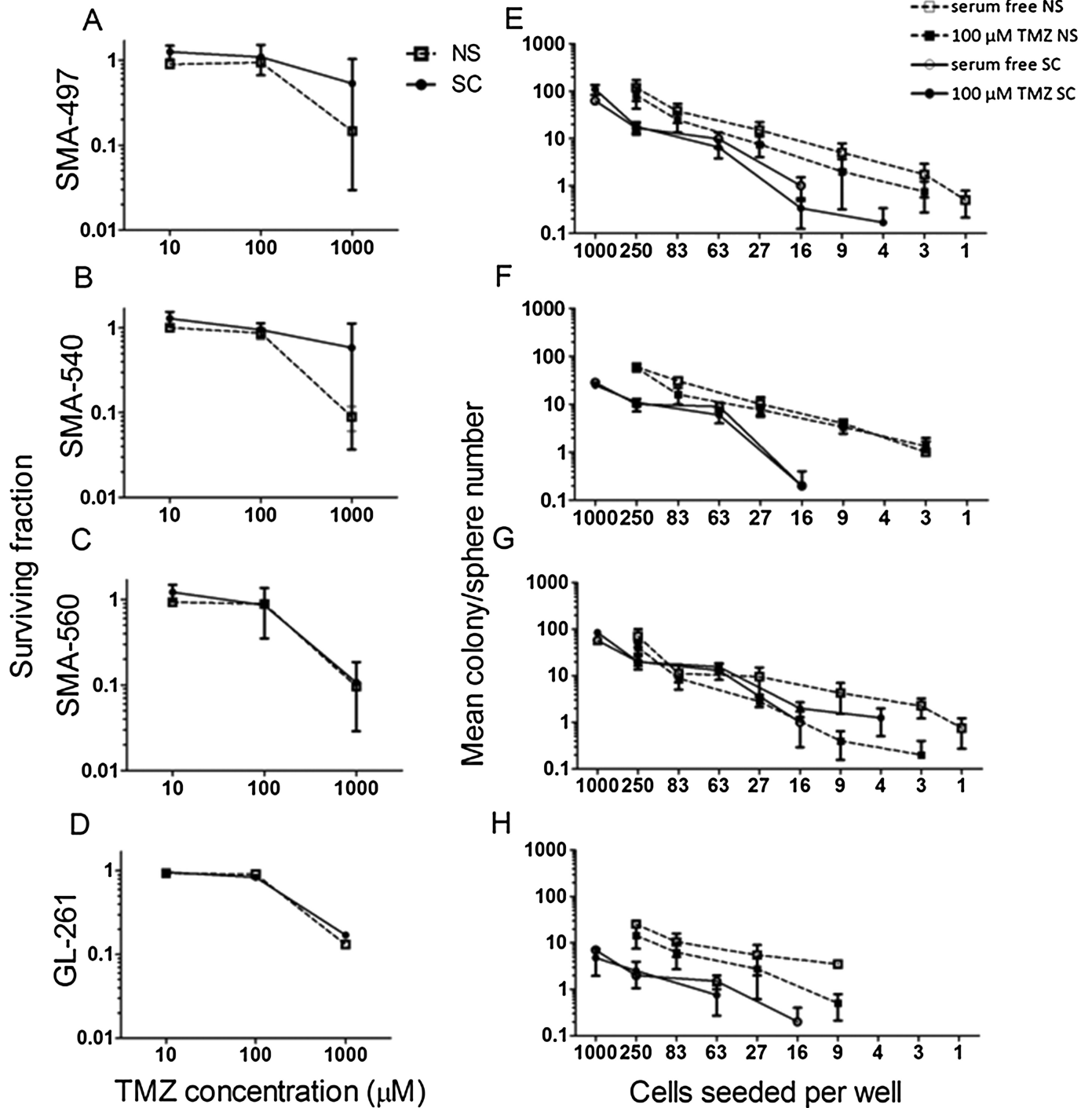


FIGURE 7. Sensitivity to temozolomide (TMZ) of nonsphere versus sphere cells in vitro. **(A–D)** The effect of increasing concentrations (0, 10, 100, 1,000 μmol/L) of TMZ on the proliferation of nonsphere cells (open squares, dotted lines) versus sphere cells (filled circles, black lines) was assessed by treating 1,000 cells plated on 96-well plates and allowing them to recover for 5 to 14 days. Assays were stopped when untreated cells became confluent. Quantification was done by alamarBlue staining (n = 3). **(E–H)** Limiting dilution assays after exposure to 100 μmol/L TMZ (closed square, dotted line for nonsphere cells; closed circle, continuous line for sphere cells) were performed and plotted against serum-free control (open squares, dotted line for nonsphere cells, open circle continuous line for sphere cells). Colonies or spheres were counted 4 to 20 days after seeding (n = 3, * p < 0.05, ** p < 0.01, *** p < 0.001, 2-way analysis of variance test). NS, nonsphere cultures; SC, sphere cultures.

increased activities of the respective genes (Figure, Supplemental Digital Content 6, part F, <http://links.lww.com/NEN/A668>).

We next assessed the ability for self-renewal in the form of adherent colonies for nonsphere cells or of sphere formation for sphere culture cells using limiting dilution assays. At similar seeding densities, all nonsphere cultures were superior at self-renewal to sphere cultures in their respective native culture conditions (Fig. 5A–D). To distinguish between impact of “cell type” (nonsphere vs sphere cultures) and impact of cell culture conditions (DM vs NB), we performed medium switch experiments in that the nonsphere cells were seeded and cultured in NB medium and the sphere cells in DM medium in the limiting dilution assays. These experiments demonstrated that the DM medium promoted colony formation of sphere cells, whereas the colony-forming capacity of nonsphere cells diminished to those of sphere cultures when maintained in NB medium (Fig. 5E–H).

Differential Sensitivity of Nonsphere Versus Sphere Cultures to Irradiation and TMZ

We next explored the differential sensitivity of nonsphere versus sphere cultures to single fractions of irradiation at 1, 3, or 9 Gy (Fig. 6) or to increasing concentrations of TMZ (Fig. 8). Effects on survival and repopulation as well as self-renewal properties were assessed using clonogenic survival and limiting dilution assays. Proliferation of all cell lines was only affected at 9 Gy. Nonsphere and sphere cultures of SMA-497 and SMA-560 were affected similarly, whereas SMA-540 sphere cultures ($p = 0.26$) and GL-261 nonsphere cultures ($p = 0.003$) were relatively more radiosensitive (Fig. 6A–D). Self-renewal of nonsphere cultures of all cell lines was more affected than that of sphere cultures across the full range of cell numbers seeded (Fig. 6E–H). Similar assays were performed to study the effect of TMZ. All cell lines were highly resistant to TMZ. At the highest TMZ concentration, the SMA-497 and SMA-540 nonsphere cells were more sensitive than the sphere cells but not to a significant extent. In contrast, no difference between nonsphere and sphere cultures emerged for SMA-560 or GL-261 (Fig. 7A–D). The self-renewal capacities of nonsphere and sphere cultures after exposure to TMZ at 100 $\mu\text{mol/L}$ were unaffected in all 4 cell lines at all seeding densities (Fig. 7E–H).

Tumorigenicity in Syngeneic Mice

To compare tumorigenicity in vivo, 1,000 nonsphere or sphere cells were injected into the right striatum of syngeneic VM/Dk mice for the SMA cell lines or of C57BL/6 mice for GL-261 cells. In 3 of 4 cell lines, nonsphere cell implantation produced higher tumor incidences and shorter survival times than sphere cell implantation; the significance levels for the differences of the estimated median survivals were SMA-497, $p < 0.0001$; SMA-540, $p = 0.0026$; and GL-261, $p = 0.0005$ (Fig. 8A, B, D). Only in the SMA-560 cell line did the sphere cell–derived tumors kill the animals earlier than nonsphere cell–derived tumors ($p < 0.0001$) (Fig. 8C). Accordingly, when early stages of tumor development were assessed at about Day

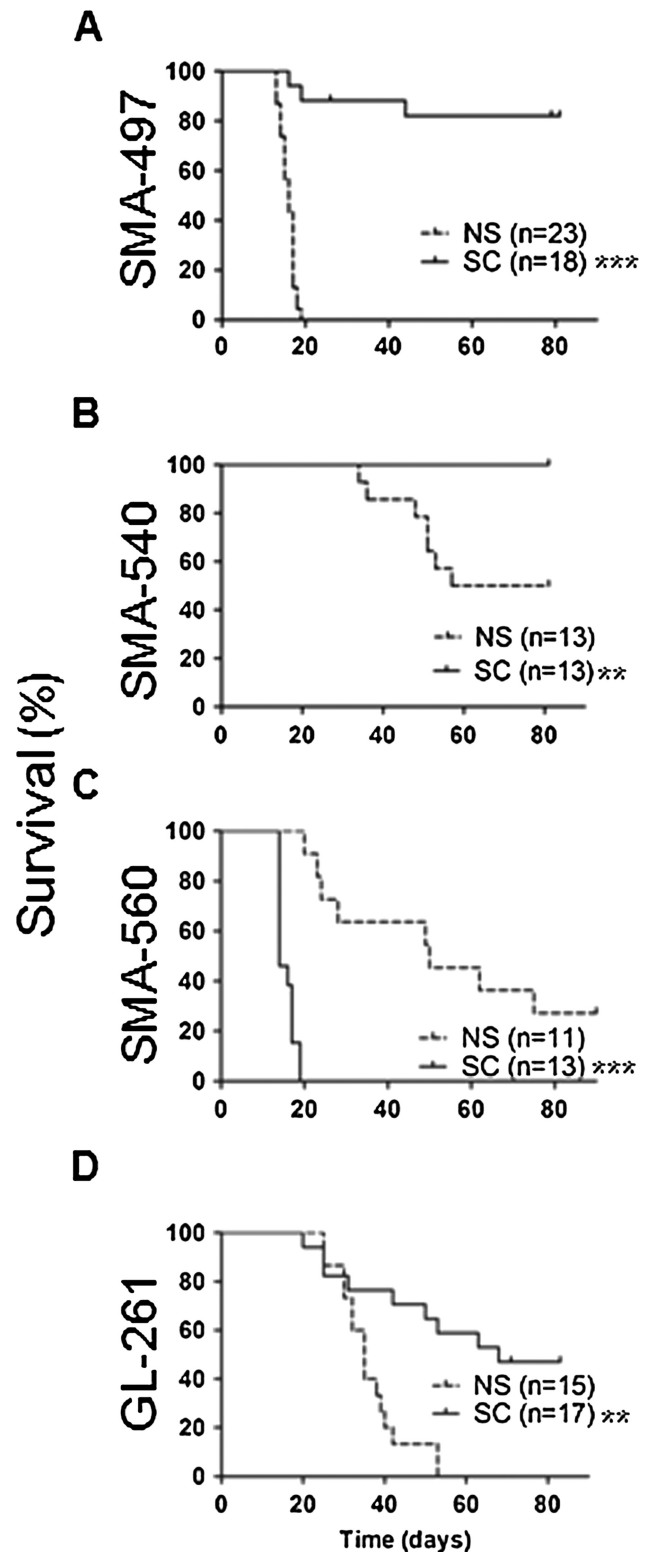


FIGURE 8. Tumorigenicity of nonsphere versus sphere cells in vivo. (A–D) One thousand nonsphere or sphere cells were implanted into the right striatum of syngeneic mice, and the mice were monitored for survival. Results were pooled from 2 separate experiments (** $p < 0.01$, *** $p < 0.001$ by logrank test). NS, nonsphere cultures; SC, sphere cultures.

14 in the SMA and at Day 29 in the GL-261 models, nonsphere cells of SMA-497 and SMA-540 and sphere cells of SMA-560 had already developed large tumors and mice showed marked clinical impairment. Tumors were rather large in GL-261 in both groups at Day 29 when the mice showed clinical disease (Table). Further tumor progression did not necessarily result in tumors with increased diameters in all groups but instead was associated with multifocal tumor formation that crossed the midline to invade into the contralateral hemisphere. Hematoxylin and eosin staining of all tumors at the terminal stage revealed a densely packed mass of pleomorphic cells. Apart from SMA-497 sphere cells, which did not form a solid primary tumor but grew diffusely from the beginning, the other nonsphere and sphere cells formed a solid lesion from which streams of tumor cells and single-cell infiltration into normal tissue evolved; this resulted in secondary tumors and proliferation around perivascular spaces distant from the primary lesion (Figure, Supplemental Digital Content 7, <http://links.lww.com/NEN/A669>). The largest tumor diameters and highest incidence of multifocal lesions were seen in the SMA-540 nonsphere and GL-261 sphere cell tumors. In end-stage tumors, proliferation assessed by Ki-67 labeling was similar in sphere and nonsphere cell-derived tumors in SMA-497 but increased in sphere cell-derived tumors of SMA-560 and GL-261. Ki-67 labeling was localized mainly at the periphery of SMA-497 nonsphere cell tumors, whereas both nonsphere and sphere cell tumors in the other cell lines had a uniform distribution of proliferating cells within the tumor.

CD44 and β IIIIT levels were assessed to explore whether some of the differences between nonsphere and sphere cultures in vitro were maintained when these cells were passaged in vivo. This was not the case because CD44 was uniformly expressed in all nonsphere and sphere culture tumors but not in the adjacent brain. In contrast, β IIIIT was barely detectable in the tumors but strongly expressed in the normal brain, corresponding to the sphere culture rather than the adherent phenotype in vitro. CD31 labeling reflecting vessel density was similar in both nonsphere and sphere cell tumors of all cell lines, with significantly higher vessel density seen in the sphere cell group only in SMA-560. The SMA-560 tumors were also the most vascularized of all models in general. CD3-labeled T cells were found localized at the tumor periphery (Figure, Supplemental Digital Content 7, part A, <http://links.lww.com/NEN/A669>) and in perivascular regions (Figure, Supplemental Digital Content 7, part C, <http://links.lww.com/NEN/A669>). They were present at higher levels in nonsphere tumors of the SMA models and in the sphere tumors of GL-261. CD11b infiltration was more prominent in nonsphere than in sphere cell tumors in the SMA models but not in GL-261 where sphere cell tumors showed higher infiltration. It was found within and outside the tumors (Figure, Supplemental Digital Content 7, part C, <http://links.lww.com/NEN/A669>) and sometimes in higher densities in areas surrounding blood vessels in GL-261 tumors (Figure, Supplemental Digital Content 7, part D, <http://links.lww.com/NEN/A669>). Overall, there was no association of the extent of immune cell infiltration with outcome.

DISCUSSION

The notion that cancers, although of monoclonal origin, are heterogeneous and not composed of a monomorphic population of cells is now widely accepted. Various approaches have been used to characterize and derive a population of cancer stem cells from various types of tumors, including brain tumors, in particular glioblastoma. These cancer stem cells have been considered an often quiescent slowly proliferating pool of cells exhibiting resistance to conventional modes of nonsurgical therapies, that is, irradiation or genotoxic pharmacotherapy. Stem cells have not only been isolated from freshly resected tumors *ex vivo* but have also been derived from long-term glioma and other cancer cell lines and have been proposed to serve as superior model systems to study the biology of disease in terms of preserving the invasive phenotype and genomic profile of the original tumor (4, 25–27).

Here, we addressed the usefulness of stem cells defined by their sphere-forming capacity in a panel of 4 long-term mouse glioma cell lines. SMA-497, SMA-540, and SMA-560 cells were generated from a spontaneous murine astrocytoma detected in a VM/Dk mouse (15, 17). GL-261 cells were derived from a tumor generated by implantation of methylcholanthrene pellets in C57BL/6 mouse brains (16, 28). Their neuroglial origin was confirmed here by the differential often coexpression of neuroglial lineage markers such as GFAP, β IIIIT, and CNPase (Fig. 4). We found that, even after decades of passaging under differentiating (serum-containing) culture conditions, all mouse glioma cell lines had retained the plasticity to grow in spheres, with the option of long-term expansion (Fig. 1A). The sphere culture transcriptomes were uniformly enriched in some stemness-associated genes, including CD44, and such changes from nonsphere to sphere cultures were mostly confirmed at the proteome level.

Upregulation of the candidate stem cell marker CD44, a cell surface adhesion protein thought to play a role in tumor progression, has been associated with increased histopathologic grade and poorer prognosis in human gliomas as well as increased cell migration and invasiveness in A172 glioma cells (29, 30). In addition, the expression of CD44 in glioma stem cells has been shown to be controlled by the transforming growth factor- β signaling pathway, which is a target for glioma therapy because of its role in tumor growth (31). Here, CD44 expression increased in 3 of 4 cell lines under sphere culture conditions, but CD44 was almost lost when SMA-540 cells were induced to assume a sphere culture phenotype (Fig. 3A). The classical glioma stem cell marker CD133, which is increasingly questioned regarding its usefulness to delineate stem cells of human glioblastomas (32–34), did not distinguish between sphere and nonsphere cultures in this panel of mouse glioma cell lines (Fig. 3B). Finally, neither nestin nor Musashi-1 expression correlated with the nonsphere versus sphere culture phenotype (Fig. 3C–F). Importantly, our study does not challenge the value of any of these markers to detect stemness because we do not propose that the sphere cultures generated by changing the culture conditions should be considered stemlike.

Glial fibrillary acidic protein, β IIIIT, and CNPase are commonly used as markers of astrocytic, neuronal, and oligodendroglial differentiation, although GFAP expression is also a radial glial neural stem cell marker (35). Our analyses of differentiated neural and glial markers showed that sphere culture conditions did not exclusively enrich for a less differentiated stemlike phenotype (as previously observed [36]), as evidenced by the expression of GFAP and CNPase. Of note, the anti-CNPase antibody used here recognizes both the 46-kDa CNPase isoform, present in mature oligodendrocytes, and the 48-kDa, both of which were found to be expressed in oligodendrocyte precursor cells in the normal rat brain as well as in C6 glioma cells (37, 38). By contrast, sphere cultures of all cell lines showed decreased expression of the mature neuronal marker β IIIIT (Fig. 4).

We found that sphere cultures have slowed growth, which we attribute to the deprivation of serum-derived mitogenic stimuli (Figure, Supplemental Digital Content 6, <http://links.lww.com/NEN/A668>). Unexpectedly, sphere cultures from all 4 cell lines displayed lower self-renewal capacity than nonsphere cultures in limiting dilution assays. Medium switch experiments disclosed that the type of medium rather than a stable sphere culture versus nonsphere trait conferred the increased self-renewal (Fig. 5).

Relative resistance to radiotherapy and chemotherapy, the principal treatment modalities for human glioblastoma patients (39), is a conceptual hallmark of glioma stem cells. Putatively related to slowed growth kinetics, sphere cultures were uniformly less radiosensitive than nonsphere cultures (Fig. 6), but both sphere and nonsphere mouse glioma cell cultures were resistant to clinically relevant concentrations of TMZ (Fig. 7).

Recent studies have highlighted the limitations of using sphere culture conditions to enrich for cancer stem cells (36, 40). In vivo studies indicated that sphere cells with low self-renewal capacity in vitro generated rapidly developing tumors with higher penetrance compared with more stemlike cells that possessed higher in vitro self-renewal capacity (41). Using a limiting cell implantation number approach to critically assess the tumorigenicity of sphere cultures versus nonsphere, we found that sphere cultures were not enriched in cells with a higher tumorigenic potential in vivo (Fig. 8). In fact, nonsphere cultures were more tumorigenic in all but the SMA-560 cell line. Moreover, we did not observe stable morphologic phenotypes defined by proliferative activity or vascular density that would have allowed distinguishing between nonsphere and sphere cell-derived tumors derived from the same cell line, suggesting that the differential culturing in vitro confirmed differential properties for initial seeding and growth in vivo but did not produce genuinely different tumors. Thus, living in a sphere rather than as a monolayer in vitro is a state rather than a trait of a mouse glioma cell. Accordingly, the differences in CD44 expression between nonsphere and sphere cultures were not maintained in vivo, and, interestingly, the loss of β IIIIT in vivo may indicate that sphere cultures are closer to the in vivo situation than nonsphere cultures. Furthermore, there also seemed to be no difference in immune responsiveness and host cell infiltration defined by the numbers of CD3-positive T cells or of CD11b-positive cells, possibly representing myeloid suppressor cells.

In conclusion, this study provides an extensive characterization of the most commonly used syngeneic mouse glioma models that should guide researchers in selecting such models for their studies. We found no evidence that studies performed with sphere cultures derived from long-term cell lines are biologically more meaningful than studies performed using standard monolayer cultures, at least in the investigated mouse glioma lines. Future studies may need to define whether this also holds true for other glioma cell line model systems. Importantly, our data must not be used to argue against the increasing use of human stemlike tumor cell lines immediately derived from freshly resected tumor specimens.

ACKNOWLEDGMENTS

The authors thank Silvia Dolski for technical support. Thorsten Wachtmeister, Genomics and Transcriptomics Laboratory, Center for Biological and Medical Research (BMFZ), Heinrich Heine University, is acknowledged for excellent support with the hybridization of Affymetrix microarrays.

REFERENCES

- Ronning PA, Helseth E, Meling TR, et al. A population-based study on the effect of temozolomide in the treatment of glioblastoma multiforme. *Neuro Oncol* 2012;14:1178–84
- Ignatova TN, Kukekov VG, Laywell ED, et al. Human cortical glial tumors contain neural stem-like cells expressing astroglial and neuronal markers in vitro. *Glia* 2002;39:193–206
- Singh SK, Hawkins C, Clarke ID, et al. Identification of human brain tumour initiating cells. *Nature* 2004;432:396–401
- Galli R, Binda E, Orfanelli U, et al. Isolation and characterization of tumorigenic, stem-like neural precursors from human glioblastoma. *Cancer Res* 2004;64:7011–21
- Eramo A, Ricci-Vitiani L, Zeuner A, et al. Chemotherapy resistance of glioblastoma stem cells. *Cell Death Differ* 2006;13:1238–41
- Liu GT, Yuan XP, Zeng ZH, et al. Analysis of gene expression and chemoresistance of CD133(+) cancer stem cells in glioblastoma. *Mol Cancer* 2006;5:67
- Bao S, Wu Q, McLendon RE, et al. Glioma stem cells promote radioresistance by preferential activation of the DNA damage response. *Nature* 2006;444:756–60
- Qiang L, Yang Y, Ma YJ, et al. Isolation and characterization of cancer stem like cells in human glioblastoma cell lines. *Cancer Lett* 2009;279:13–21
- Shen G, Shen F, Shi ZJ, et al. Identification of cancer stem-like cells in the C6 glioma cell line and the limitation of current identification methods. *In Vitro Cell Dev-An* 2008;44:280–89
- Zhou XD, Wang XY, Qu FJ, et al. Detection of cancer stem cells from the C6 glioma cell line. *J Int Med Res* 2009;37:503–10
- Muto J, Imai T, Ogawa D, et al. RNA-binding protein Musashi1 modulates glioma cell growth through the post-transcriptional regulation of Notch and PI3 kinase/Akt signaling pathways. *PLoS One* 2012;7:10
- Pellegatta S, Poliani PL, Corno D, et al. Neurospheres enriched in cancer stem-like cells are highly effective in eliciting a dendritic cell-mediated immune response against malignant gliomas. *Cancer Res* 2006;66:10247–52
- Wu A, Oh S, Wiesner SM, et al. Persistence of CD133+ cells in human and mouse glioma cell lines: Detailed characterization of GL261 glioma cells with cancer stem cell-like properties. *Stem cells and development* 2008;17:173–84
- Huszthy PC, Daphu I, Niclou SP, et al. In vivo models of primary brain tumors: Pitfalls and perspectives. *Neuro Oncol* 2012;14:979–93
- Serano RD, Pegram CN, Bigner DD. Tumorigenic cell culture lines from a spontaneous VM/Dk murine astrocytoma (SMA). *Acta Neuropathol* 1980;51:53–64
- Ausman JI, Shapiro WR, Rall DP. Studies on the chemotherapy of experimental brain tumors: Development of an experimental model. *Cancer Res* 1970;30:2394–400

17. Fraser H. Astrocytomas in an inbred mouse strain. *J Pathol* 1971;103:266–70
18. Binder H, Krohn K, Preibisch S. “Hook”-calibration of GeneChip-microarrays: Chip characteristics and expression measures. *Algorithms Mol Biol* 2008;3:11
19. Irizarry RA, Hobbs B, Collin F, et al. Exploration, normalization, and summaries of high density oligonucleotide array probe level data. *Bio-statistics* 2003;4:249–64
20. Wirth H, Löffler M, von Bergen M, et al. Expression cartography of human tissues using self organizing maps. *BMC Bioinformatics* 2011;12:306
21. Hopp L, Wirth H, Fasold M, et al. Portraying the expression landscapes of cancer subtypes: A glioblastoma multiforme and prostate cancer case study. *Systems Biomed* 2013;1:99–121
22. Wirth H, von Bergen M, Binder H. Mining SOM expression portraits: Feature selection and integrating concepts of molecular function. *BioData Mining* 2012;5:18
23. Wirth H, von Bergen M, Murugaiyan J, et al. MALDI-typing of infectious algae of the genus *Prototheca* using SOM portraits. *J Microbiol Methods* 2012;88:83–97
24. Wang X. Computational analysis of expression of human embryonic stem cell-associated signatures in tumors. *BMC Res Notes* 2011;4:471
25. Li A, Walling J, Kotliarov Y, et al. Genomic changes and gene expression profiles reveal that established glioma cell lines are poorly representative of primary human gliomas. *Mol Cancer Res* 2008;6:21–30
26. Ernst A, Hofmann S, Ahmadi R, et al. Genomic and expression profiling of glioblastoma stem cell-like spheroid cultures identifies novel tumor-relevant genes associated with survival. *Clin Cancer Res* 2009;15:6541–50
27. Schulte A, Gunther HS, Phillips HS, et al. A distinct subset of glioma cell lines with stem cell-like properties reflects the transcriptional phenotype of glioblastomas and overexpresses CXCR4 as therapeutic target. *Glia* 2011;59:590–602
28. Zimmerman HM, Arnold H. Experimental brain tumors: II. Tumors produced with benzpyrene. *Am J Pathol* 1943;19:939–55
29. Yoshida T, Matsuda Y, Naito Z, et al. CD44 in human glioma correlates with histopathological grade and cell migration. *Pathol Int* 2012;62:463–70
30. Wei KC, Huang CY, Chen PY, et al. Evaluation of the prognostic value of CD44 in glioblastoma multiforme. *Anticancer Res* 2010;30:253–59
31. Anido J, Saez-Borderias A, Gonzalez-Junca A, et al. TGF-beta receptor inhibitors target the CD44(high)/Id1(high) glioma-initiating cell population in human glioblastoma. *Cancer Cell* 2010;18:655–68
32. Sun Y, Kong W, Falk A, et al. CD133 (Prominin) negative human neural stem cells are clonogenic and tripotent. *PLoS One* 2009;4:e5498
33. Joo KM, Kim SY, Jin X, et al. Clinical and biological implications of CD133-positive and CD133-negative cells in glioblastomas. *Lab Invest* 2008;88:808–15
34. Beier D, Rohrl S, Pillai DR, et al. Temozolomide preferentially depletes cancer stem cells in glioblastoma. *Cancer Res* 2008;68:5706–15
35. Doetsch F, Caille I, Lim DA, et al. Subventricular zone astrocytes are neural stem cells in the adult mammalian brain. *Cell* 1999;97:703–16
36. Pollard SM, Yoshikawa K, Clarke ID, et al. Glioma stem cell lines expanded in adherent culture have tumor-specific phenotypes and are suitable for chemical and genetic screens. *Cell Stem Cell* 2009;4:568–80
37. Gravel M, Gao E, Hervouet-Zeiber C, et al. Transcriptional regulation of 2',3'-cyclic nucleotide 3'-phosphodiesterase gene expression by cyclic AMP in C6 cells. *J Neurochem* 2000;75:1940–50
38. Scherer SS, Braun PE, Grinspan J, et al. Differential regulation of the 2',3'-cyclic nucleotide 3'-phosphodiesterase gene during oligodendrocyte development. *Neuron* 1994;12:1363–75
39. Weller M, van den Bent M, Hopkins K, et al. EANO guideline for the diagnosis and treatment of anaplastic gliomas and glioblastoma. *Lancet Oncol* 2014;15:e395–403
40. Pastrana E, Silva-Vargas V, Doetsch F. Eyes wide open: A critical review of sphere-formation as an assay for stem cells. *Cell Stem Cell* 2011;8:486–98
41. Barrett LE, Granot Z, Coker C, et al. Self-renewal does not predict tumor growth potential in mouse models of high-grade glioma. *Cancer Cell* 2012;21:11–24

Supplementary Methods

Gene expression profiling

Extraction of total RNA from cell pellets was performed with the RNeasy Mini Kit from Qiagen (Hilden, Germany). RNA integrity was checked with the Agilent 2100 BioAnalyzer. Sample preparation was done with 100 ng total RNA using the Ambion[®] WT Expression Kit from Applied Biosystems (PN 4411973, Life Technologies, Invitrogen) and the Gene Chip[®] WT Terminal Labeling and Controls Kit (PN 901525) from Affymetrix (Santa Clara, CA) according to the instructions of the Ambion[®] WT Expression Kit Manual (PN 4425209 Rev C) and the Gene Chip[®] WT Terminal Labeling and Hybridization User Manual (PN 702808 Rev 7). A total of 5 µg of the labeled cDNA were hybridized to the Gene Chip[®] Mouse Gene 1.0 ST Array (Affymetrix, PN 901168) at the Center for Biological and Medical Research at Heinrich Heine University Düsseldorf.

Proteomics

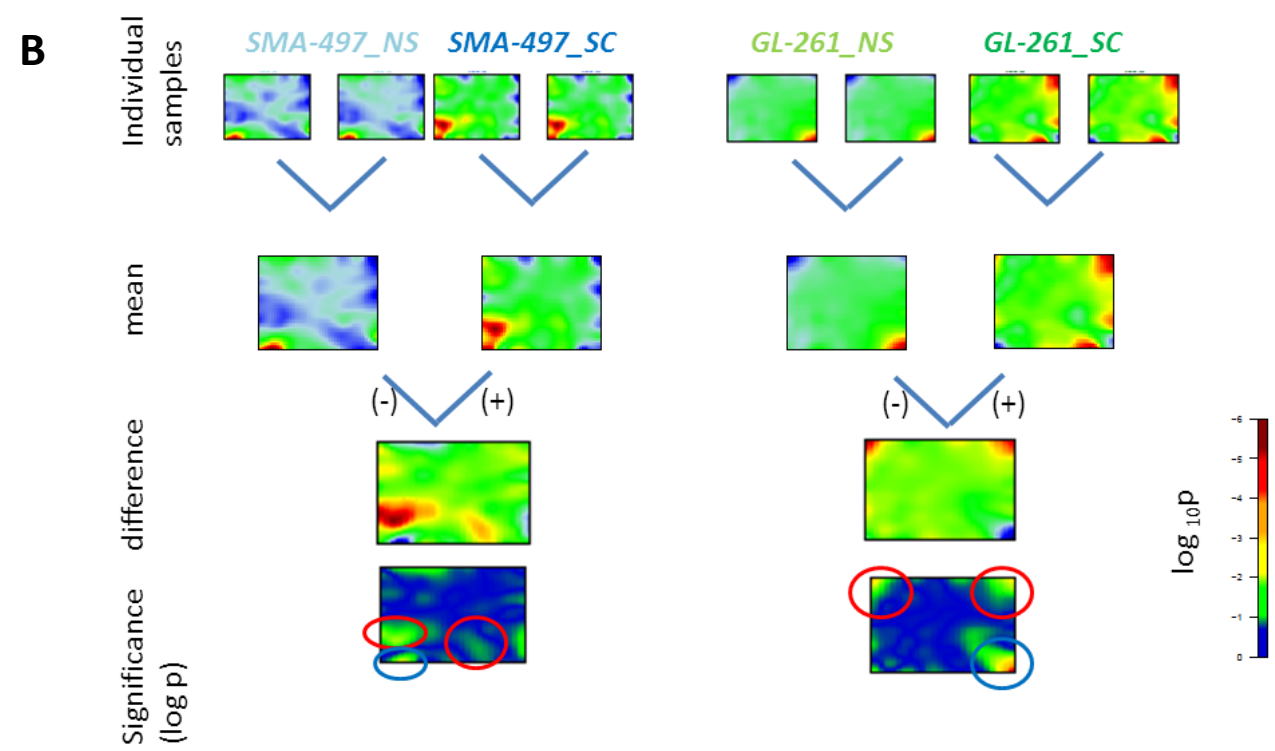
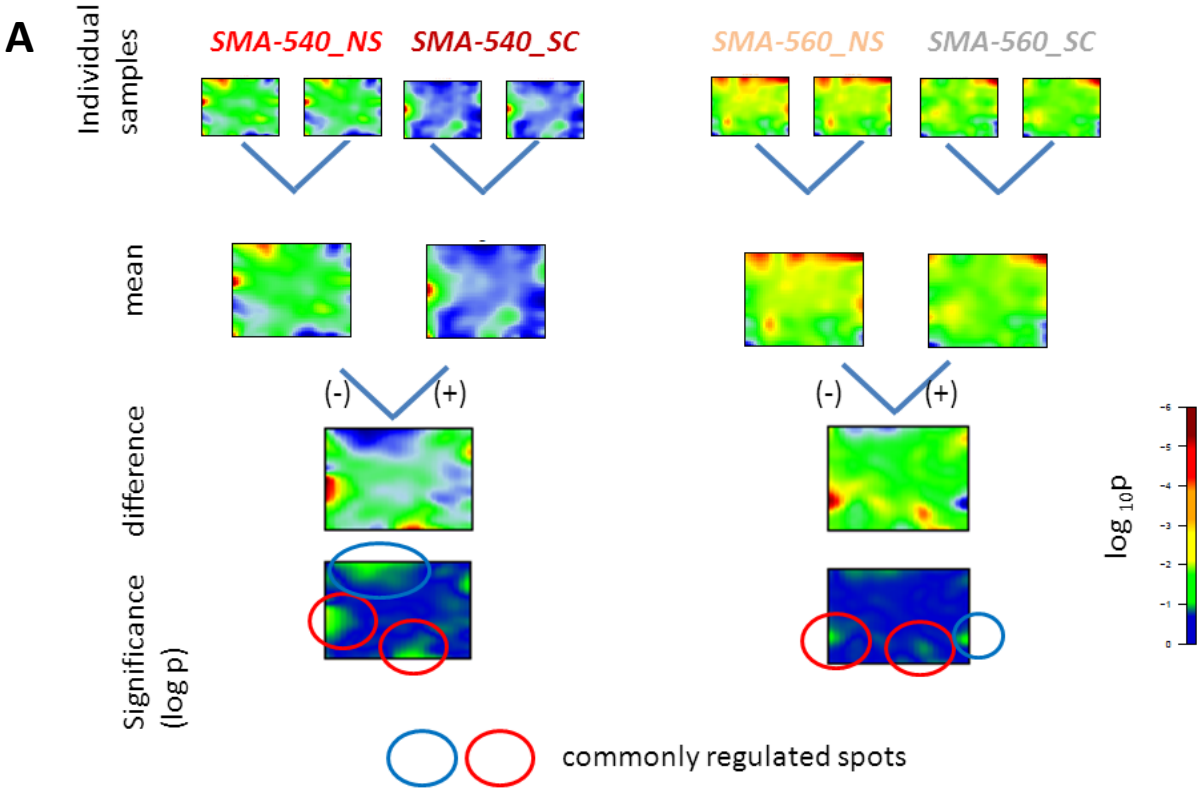
For proteome analysis 100 µg cell pellets were homogenized in 500 µl lysis buffer (30 mM Tris, 7 M Urea, 2 M Thiourea, 4% 3-[(3-cholamidopropyl)dimethylammonio]-1-propanesulfonate (CHAPS); pH 8.5). Subsequently, total protein amounts were determined using BCA protein assays (Thermo Scientific Pierce, Rockford, IL, USA) and 10 µg of each sample were loaded onto a SDS-PAGE gel (Life Technologies, Darmstadt, Germany). After complete entry into the gel, the electrophoresis was stopped and the gel was stained with coomassie (1). Briefly, gel bands were cut out, alternately washed with 10 mM NH₄HCO₃ and 10 mM NH₄HCO₃ /Acetonitrile (50% v/v) followed by tryptic digestion (sequencing grade modified trypsin, Promega, Mannheim, Germany) over night at 37°C. Mass spectrometric analyses of whole cell lysates were carried out using a label-free MS approach for quantification. Extracted peptides were analyzed with a nano-HPLC/ESI-MS system (RSLCnano[™] U3000

HPLC, Thermo Fisher Scientific, Bremen, Germany) online coupled with a LTQ Orbitrap EliteTM (Thermo Fisher Scientific) mass spectrometer equipped with a nano-electrospray ion source (nano-ESI). 300 ng of each sample were loaded onto a C₁₈ trapping column (Acclaim PepMap C₁₈, 2 cm × 100 μm × 5 μm, 100 Å, Thermo Fisher Scientific) and desalted with 0.1% trifluoroacetic acid (TFA) for 10 min. Peptides were eluted from the trap column and subsequently separated using an analytical column (Acclaim PepMap RSLC C₁₈; 25 cm × 75 μm × 2 μm, 100 Å, Thermo Fisher Scientific) for 120 min with a flow rate of 300 nL/min before spraying into the MS. The mobile phase for chromatography consisted of 0.1% formic acid in water (solvent A) and 84% acetonitrile, 0.1% formic acid in water (solvent B). The gradient started with 4% B, ramped to 10% B in 5 min, 20% B in 62 min, 30% B in 35 min, 40% B in 15 min and 95% B in 2 min. System parameters were as follows: spray voltage, 1.4 kV; ion transfer tube temperature, 275 °C; collision gas, helium; collision gas pressure, 1.3 mTorr; normalized collision energy for tandem spectroscopy (MS/MS), 35%. The Orbitrap Elite was operated in a TOP20 data-dependent mode to automatically switch between MS and MS/MS acquisition. MS-spectra were acquired in the Orbitrap with a mass range of 350-1700 m/z and a resolution of 60,000. Polysiloxane (445.120030 Th) was used as lock mass. For MS/MS, ions were isolated with an isolation width of 2 m/z and fragmented using collision-induced dissociation (CID). MS/MS-spectra were acquired in the linear ion trap in centroid mode. Target ions selected for MS/MS were dynamically excluded for 45 sec. The ion selection threshold for MS/MS was 500 counts. For protein identification Proteome DiscovererTM (version 1.3, Thermo Fisher Scientific) and MASCOTTM search engine (version 2.4.1, Matrix Science, London, UK) were used. MS/MS-spectra were searched against the UniProtKB/Swiss-Prot database (16608 mouse sequences; date 04/03/2013). Search parameters were as follows: enzyme: trypsin; 2 maximum missed cleavage sites;

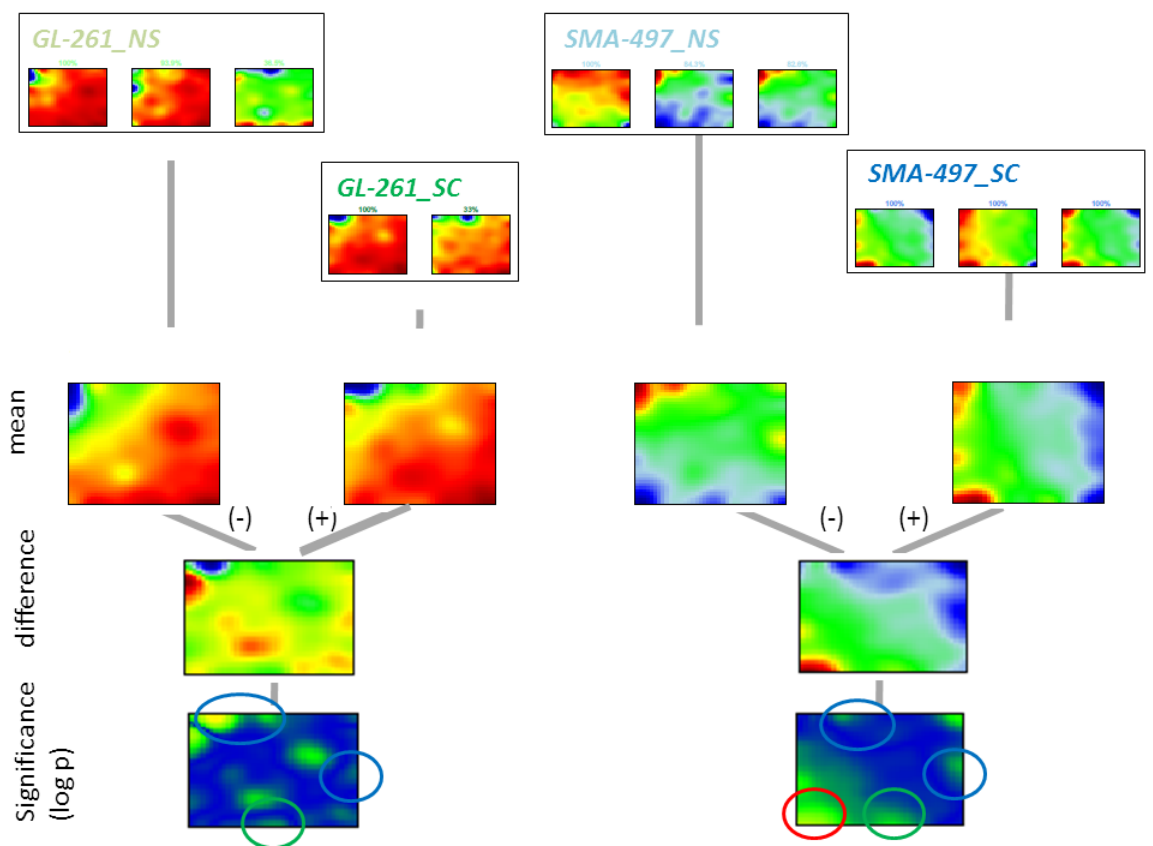
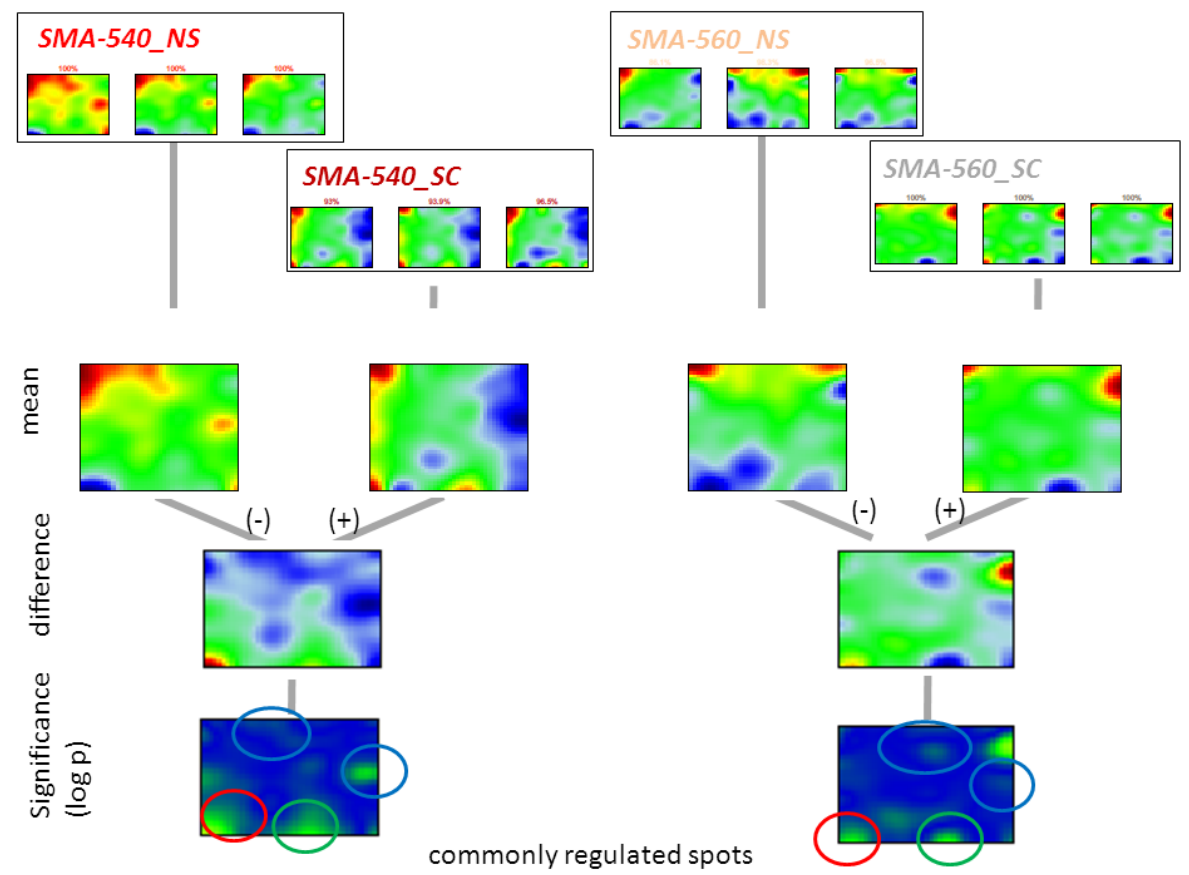
taxonomy: mus musculus; 10 ppm precursor mass tolerance; 0.4 Da fragment mass tolerance; oxidation of methionine as dynamic modification; carbamidomethylation of cysteine as fixed modification. The false discovery rate (FDR) was set to 1% ($p \leq 0.01$). If identified peptides are shared between two proteins, these are combined and reported as one protein group. Label-free quantification was carried out using ProgenesisTM LC-MS (Nonlinear Dynamics, Newcastle upon Tyne, UK) (2). A minimum of two unique peptides were required for quantification. Proteins with a significant (anova <0.01) abundance change of 2.0 were considered as differentially regulated. Proteins with less than two quantifiable peptides were excluded.

Supplementary References

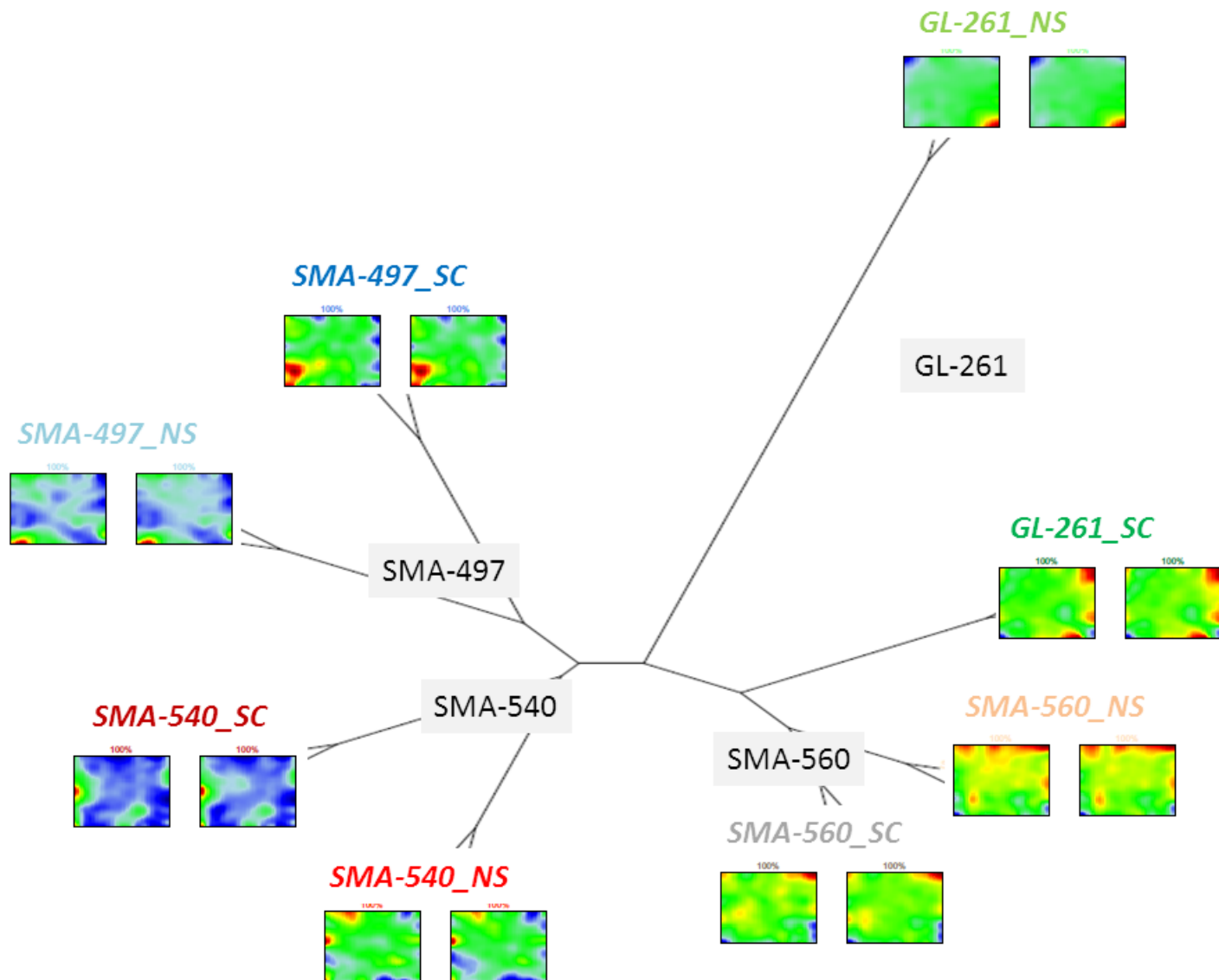
1. Neuhoff V, Arold N, Taube D, et al. Improved staining of proteins in polyacrylamide gels including isoelectric focusing gels with clear background at nanogram sensitivity using Coomassie Brilliant Blue G-250 and R-250. *Electrophoresis* 1988;9;255-62.
2. Sitek B, Waldera-Lupa DM, Poschmann G, et al. Application of label-free proteomics for differential analysis of lung carcinoma cell line A549. *Methods in molecular biology* 2012;893;241-8.



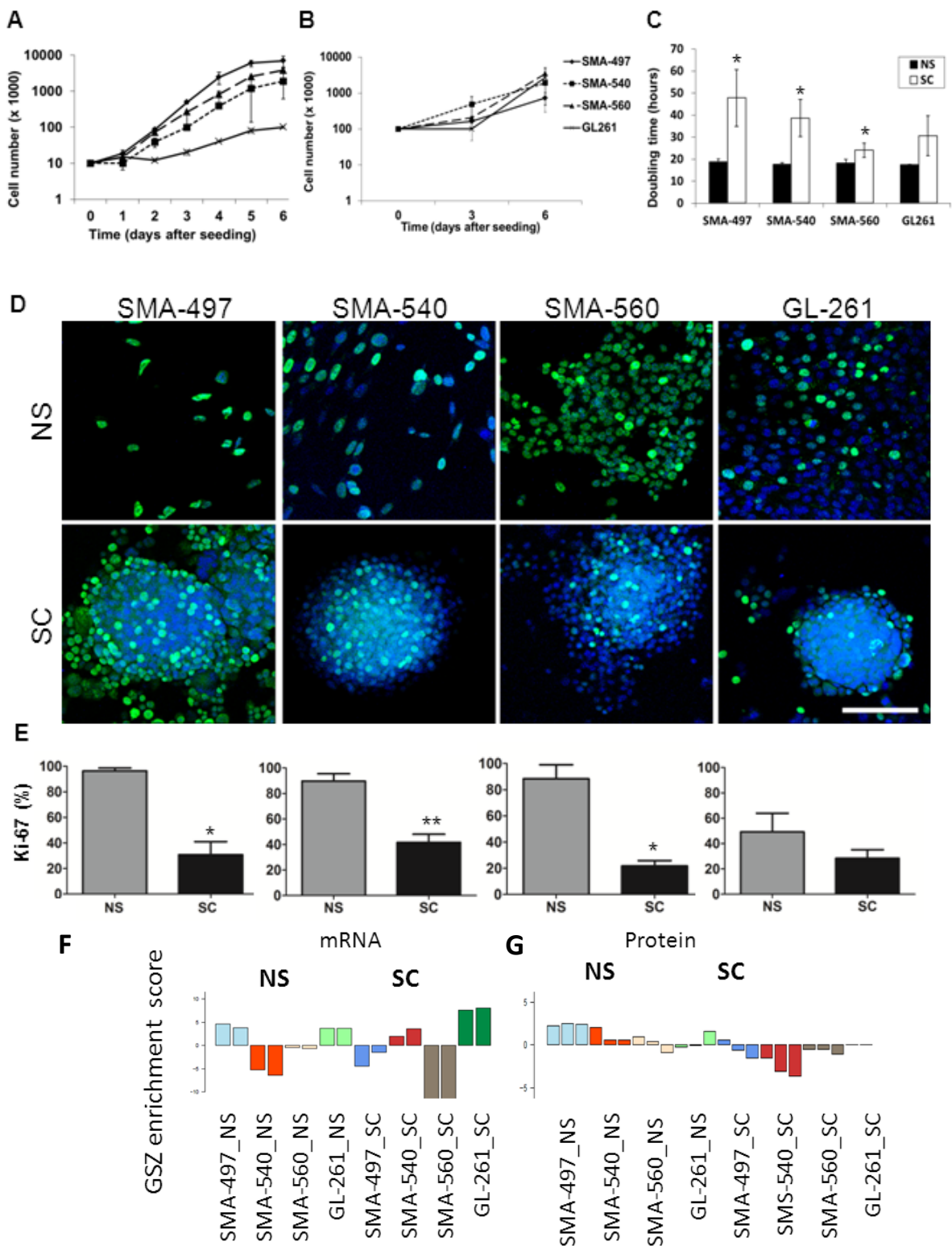
Suppl. Figure 1A, B: Processing steps of SOM analysis - Transcriptomics. Expression levels of the 20,000 genes in each sample is characterized by one SOM portrait (upper row of images). The images of the replicates are averaged. Their mean portrait characterizes each condition (second row). The differences between the mean portraits of the non-sphere and the sphere conditions provide the difference portrait of each cell line (third row). The coloring of the portraits refers to the log expression scale of the genes. The significance portraits provide significance of differential expression in units of log p-values using a moderate t-test. The red and blue ellipses indicate clusters of significantly and consistently differentially expressed genes.

A**B**

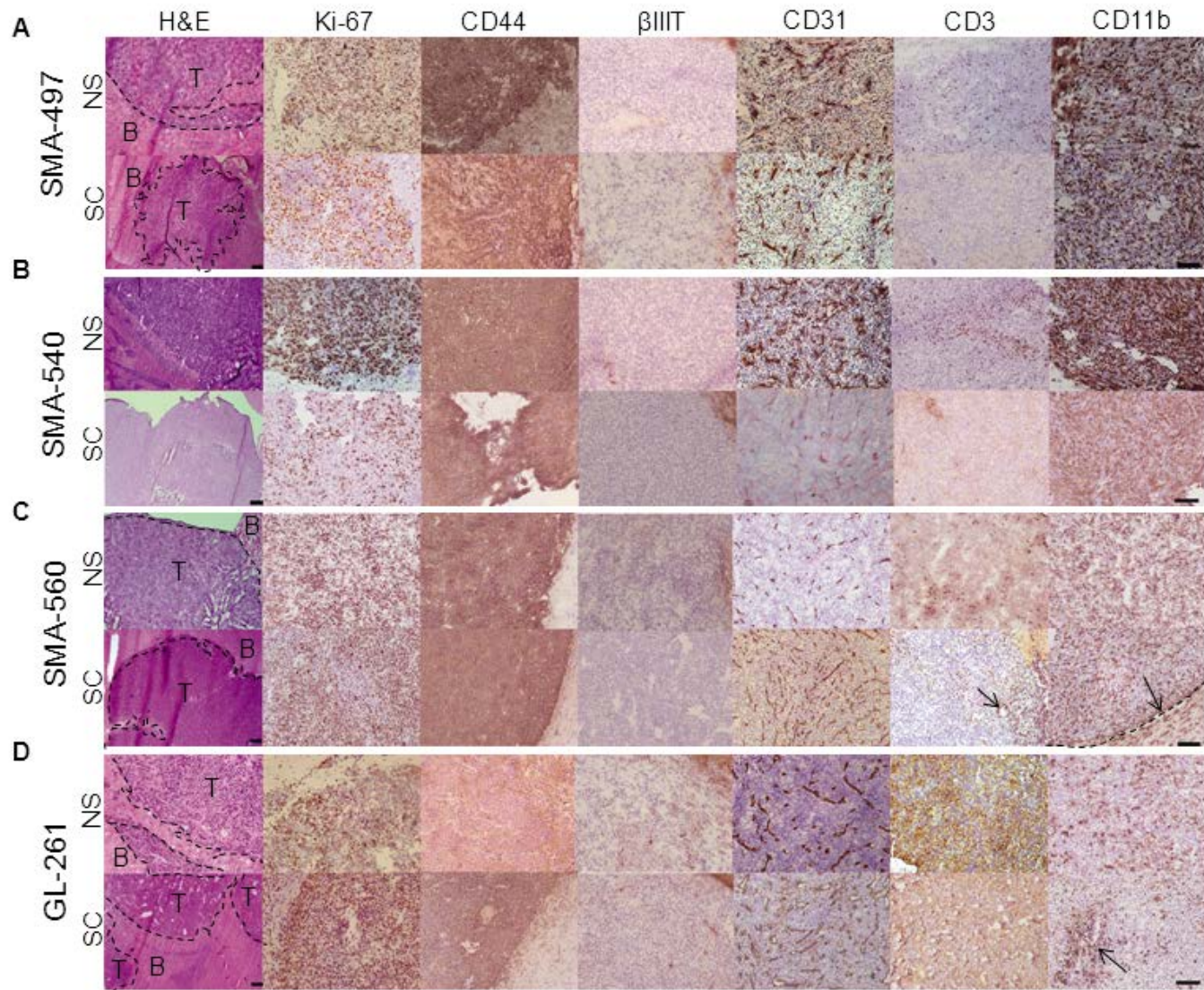
Suppl. Figure 2A, B: Processing steps of SOM analysis - Proteomics. See legend to Supplementary Figure 1 for details.



Suppl. Figure 3. Similarity tree of the SOM expression landscapes of all samples studied. Note that the 2 replicates measured at each condition arrange as twins at the end of one of the branches. Samples of the same cell line cultured under non-sphere and sphere conditions merge on the next level of branching. This hierarchy of similarity indicates that the expression landscapes are dominated by cell line characteristics.



Suppl. Figure 5. Non-sphere vs. sphere cell proliferation in vitro. A, B: Growth of non-sphere (A) or sphere (B) cells was monitored over 6 d using trypan blue cell dye exclusion to quantify viable cells in 3 separate experiments. C: Data from A and B were used to derive doubling times (* $P < 0.05$, paired student t-test). D, E: Ki-67 was detected by immunofluorescence microscopy (D) and quantified from 3 staining experiments. Scale bars for fluorescent images in D, 50 μm . Quantification in E was done using DAPI counterstaining (* $P < 0.05$, ** $P < 0.01$, paired t-test with equal variance). F, G. Differential expression of the cell division marker set derived from gene ontology between non-sphere and sphere cells on mRNA and protein level (<http://www.broadinstitute.org/gsea>).



Suppl. Figure 6. Tumorigenicity of non-sphere vs. sphere cells in vivo. A-D. Light microscopy images showing hematoxylin and eosin (H&E) staining at 2.5x magnification and Ki-67, CD44, β IIIIT, CD31, CD3 and CD11b immunostaining of non-sphere (upper rows) vs. sphere (lower row) cell-derived tumors at 10x magnification. Size bars correspond to 100 μ m. The tumors (T) in the H&E stainings are indicated by the black dashed lines within the surrounding normal brain tissue (B). Arrows indicate the accumulation of T cells (CD3) and macrophages (CD11b) at tumor periphery and around blood vessels.